Gneiss domes, vertical and horizontal mass transfer, and the initiation of extension in the hot lower-crustal root of a continental arc, Fiordland, New Zealand

Keith A. Klepeis[1], Joshua Schwartz[2], Harold Stowell[3], and Andrew Tulloch[4]
[1]DEPARTMENT OF GEOLOGY, UNIVERSITY OF VERMONT, BURLINGTON, VERMONT 05405-0122, USA
[2]DEPARTMENT OF GEOLOGICAL SCIENCES, CALIFORNIA STATE UNIVERSITY–NORTHRIDGE, NORTHRIDGE, CALIFORNIA 91330, USA
[3]DEPARTMENT OF GEOLOGICAL SCIENCES, UNIVERSITY OF ALABAMA, TUSCALOOSA, ALABAMA 35487, USA
[4]GNS SCIENCE, DUNEDIN, NEW ZEALAND

ABSTRACT

Structural analyses and sensitive high-resolution ion microprobe–reverse geometry (SHRIMP-RG) zircon $^{206}Pb/^{238}U$ dates reveal the tectonic evolution of the deep (40–65 km) root of a Cretaceous continental arc as subduction beneath Gondwana ended and rifting began. By ca. 123 Ma, a dense root, composed partly of garnet pyroxenite and omphacite granulite, had formed. At 118–115 Ma, during regional contraction, a magma flare-up thermally and mechanically rejuvenated the base of the arc, resulting in widespread crustal melting, granulite-facies metamorphism, and the circulation of hot partially molten lower crust. By ca. 114 Ma, the flow formed two different styles of migmatitic gneiss domes. At the deepest (~65 km) levels, the Breaksea domes record the upward flow of material in diapirs balanced by a sinking garnet pyroxenite root. At shallower (~40 km) levels, the Malaspina domes record lateral flow in 1–2-km-thick channels beneath a roof of Paleozoic gneiss. At ca. 106 Ma, regional extension began with the formation of the Doubtful Sound shear zone (106–97 Ma), followed by the Resolution Island shear zone (95–89 Ma). These structures overprint migmatitic fabrics in the gneiss domes and record lower-crustal thinning, decompression with cooling (<730 °C), and horizontal flow oblique to the arc. They also show a migration of deformation toward the Gondwana interior that was driven by differences in the thermal structure and viscosity of the lower crust. In our model, gneiss doming and root detachment were precursors to rifting and triggered by magmatism. The evolution of extension occurred in three stages that reflect both the rheological structure of the lower crust and the influence of propagating spreading ridges.

LITHOSPHERE GSA Data Repository Item 2016032 doi:10.1130/L490.1

INTRODUCTION

Studies of continental arc roots are essential to our understanding of orogenesis, batholith construction, and the evolution of continental lithosphere. Over the past two decades, the lower crust and upper mantle of arcs have attracted considerable attention, mainly because these layers are conduits for the transfer of mass and heat through the lithosphere (e.g., Kay and Kay, 1993; Saleeby et al., 2003; Hacker et al., 2015). In addition, lower-crustal melting, assimilation, storage, and homogenization (MASH) domains greatly influence the evolution and diversification of arc magmas (Hildreth and Moorbath, 1988; Jagoutz and Kelemen, 2015). Key questions center on (1) the time scales of magma flare-ups and their relationship to batholith construction, (2) how the rheological and compositional structures of arc roots change through time, (3) the types and origins of mass-transfer mechanisms in the deep crust, and (4) the consequences of these processes for arc evolution. Ultimately, establishing the linkages among these elements will improve our understanding of the rates and mechanisms by which continents grow and crustal material is recycled at convergent margins.

One of the most challenging aspects of studying arc roots involves determining the evolution of its physical, chemical, and rheological structures. Much of what is known is inferred indirectly from xenoliths (Ducea, 2002; Chin et al. 2013), exposures of high-pressure (0.8–1.2 GPa) metamorphic terrains (Miller et al., 2009; Jagoutz and Behn, 2013), geophysical experiments (Huang et al., 2013), and experiments that simulate deep crustal partial melting and fractional crystallization processes (Getsinger et al., 2009). These and other studies have identified many of the ways in which the strength, composition, and physical properties of arc roots change, including by the addition or removal of material and heat. However, there is still uncertainty over the dimensions, durations, and effects of competing processes (e.g., Ducea et al., 2015b; Hacker et al., 2015; Jagoutz and Kelemen, 2015). Part of the problem is that few places expose large (>1000 km^2) tracts of lower crust from depths >35 km, and even fewer areas have yielded precise information on the scales and rates of events at these depths. This paucity of information hinders our understanding of arc evolution.

Ascertaining the significance of deformation in the deep crust is equally challenging. Most arcs, for example, record cycles of thickening and extension that can result from multiple causes (DeCelles et al., 2009; Cao et al., 2015). If convergence stops, or basal tractions are reduced, gravitational potential energy and pressure gradients can drive both lateral and vertical flow (Godin et al., 2006; Rey et al., 2009, 2011; Jamieson and Beaumont, 2011). In arcs with thick hot crust, density contrasts may result in the viscous removal of material from the root (Kay and Kay, 1993; Saleeby et al., 2003; Lee et al., 2014; Jagoutz and Kelemen, 2015). Other types of buoyancy-driven flow also appear likely, either in channels or in diapirs (Whitney et al., 2004; Betka and Klepeis, 2013; Kruckenberg et al., 2013; Hacker et al., 2015). In effect, the types and origins of these mass-transfer mechanisms are functions of both the force balance driving the deformation and the local rheological structure. Resolving them is important because they facilitate the transfer of material and heat into and out of lower-crustal MASH zones.

In this paper, we present the results of structural analyses and U-Pb zircon sensitive high-resolution ion microprobe–reverse geometry (SHRIMP-RG) dates in a >1000 km^2 section of deeply exhumed (40–65 km) Cretaceous lower crust exposed in west-central Fiordland, New Zealand. This section once resided in a long-lived Carboniferous–Cretaceous arc on the Gondwana margin (Fig. 1). By the end of the Early Cretaceous, the arc had achieved crustal thicknesses in excess of 65 km and formed a root composed partly of garnet pyroxenite and omphacite granulite (Allibone et al., 2009c; De Paoli et al., 2009; Clarke et al., 2013). At the height of its thickness, a burst of mafic-intermediate magmatism resulted in crustal melting and granulite-facies metamorphism (Oliver, 1977; Bradshaw, 1990; Allibone et al., 2009a; De Paoli et al., 2009; Stowell et al., 2014), accompanied by the formation of migmatitic shear zones (Klepeis et al., 2007; Betka and Klepeis, 2013). These events, and subsequent cooling (Flowers et al., 2005; Schwartz et al., 2016), coincided with a regional tectonic transition as subduction and crustal thickening gave way to crustal thinning and extension, eventually leading to the breakup of Gondwana (Mortimer, 2008; Tulloch et al., 2009).

We used this setting to achieve the following goals: (1) document the three-dimensional structure of the deep (40–65 km) root of the Cretaceous arc and show how it changed over an ~35 m.y. period (123–88 Ma), (2) infer the evolution of lateral strength gradients and rheological contrasts following a short (3–4 m.y.) high-flux igneous event, (3) document the types of vertical and horizontal flow that circulated hot, partially molten material in a lower-crustal MASH zone following this flare-up, and interpret their origins, and (4) determine the spatial and temporal patterns of deformation that record the transition from crustal thickening to crustal extension. These topics are discussed in the context of new maps and cross sections (Figs. 2–5) and a three-stage sequence of events (D_1–D_3) that incorporates new structural data and $^{206}Pb/^{238}U$ zircon dates and integrates them with published pressure-temperature data and geochronology.

GEOLOGICAL CONTEXT AND PREVIOUS WORK

New Zealand now lies within a fragment of continental crust, termed Zealandia by Luyendyk (1995), that formed part of the convergent margin of Gondwana (Fig. 1) prior to the Late Cretaceous (Mortimer, 2008). The part of this orogen now exposed in Fiordland includes the Median Batholith, which records a Devonian–Early Cretaceous history of subduction and arc magmatism (Mortimer et al., 1999). The eastern (outboard) part of the batholith contains Jurassic (250–137 Ma) and older rocks that accreted onto Gondwana by ca. 129 Ma (Tulloch and Kimbrough, 2003; Marcotte et al., 2005; McCoy-West et al., 2014). The western (inboard) part includes 125–115 Ma plutons of the Western Fiordland orthogneiss (Bradshaw, 1990). Some 35% of this latter, inboard belt contains high-pressure metamorphic mineral assemblages of the garnet granulite, omphacite granulite, and eclogite facies (Turnbull et al., 2010).

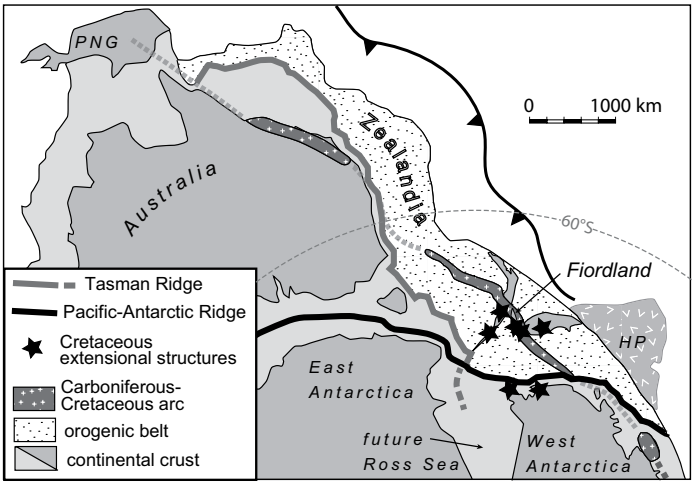

Figure 1. Tectonic reconstruction of Zealandia at ca. 90 Ma, prior to the extensional breakup of Gondwana (modified from Mortimer, 2008). HP—Hikurangi Plateau, PNG—Papua New Guinea.

Allibone et al. (2009c) subdivided the Western Fiordland orthogneiss into several large intrusions of mostly dioritic to monzodioritic composition. In the study area (Fig. 2), the oldest is the Breaksea orthogneiss, which consists of light-colored monzodioritic and monzogabbroic rock interlayered with dark layers of garnet pyroxenite, harzburgite, and hornblende peridotite (De Paoli et al., 2009). This unit was emplaced at depths of >65 km (1.8–2.0 GPa; De Paoli et al., 2009; Clarke et al., 2013). The Resolution orthogneiss and Malaspina pluton (Fig. 2) are composed mostly of hornblende diorite that was emplaced into the Breaksea orthogneiss at depths ranging from 40 to 50 km (~1.4 GPa; Allibone et al., 2009c). The Malaspina pluton is mostly 118–115 Ma but also has yielded older (ca. 120 Ma) zircon ages (Klepeis et al., 2007; Sadorski et al., 2013; Stowell et al., 2014). The age of the Resolution orthogneiss is ca. 115 Ma (Hout et al., 2012). Both units were emplaced approximately at the same time as the Misty pluton (Fig. 2), which also is dominated by hornblende diorite and was emplaced mostly at 118–115 Ma (Sadorski, 2015).

Contact relationships and metamorphic minerals show that the Malaspina pluton intruded continental margin assemblages of the Paleozoic Deep Cove gneiss after it was buried to lower-crustal depths (40–50 km; Oliver and Coggon, 1979; Allibone et al., 2009b; Daczko et al., 2009; Stowell et al., 2014). In its northern and central sectors, both the pluton and its host rock are cut by the Doubtful Sound shear zone (Figs. 4 and 5), which records extension and metamorphism at upper amphibolite facies (Gibson et al., 1988) after ca. 111 Ma (Klepeis et al., 2007). Farther west, the Resolution Island shear zone (Figs. 4 and 5) cuts the Breaksea and Resolution orthogneisses and also records extension and metamorphism at upper-amphibolite-facies conditions (Allibone et al., 2009c; Betka and Klepeis, 2013). Both shear zones postdate earlier periods of metamorphism and deformation at the granulite facies. Klepeis et al. (2007) and Stowell et al. (2014) suggested that the extension could have begun shortly following emplacement of the 118–115 Ma Malaspina pluton. However, the timing of this event is poorly known.

Extensional features within Zealandia became widespread after 105–100 Ma (Bradshaw, 1989; Mortimer, 2008; Tulloch et al., 2009, and references therein). By ca. 83 Ma, seafloor spreading in the Tasman Sea had begun (Gaina et al., 1998). Later, during the Cenozoic, the Australian-Pacific plate boundary reorganized south of New Zealand. Subduction initiated offshore of Fiordland in the Miocene, followed by strike-slip motion on the Alpine fault (Walcott, 1998; Sutherland et al., 2006).

STRUCTURAL ANALYSES AND RELATIVE CHRONOLOGY OF EVENTS

Methods

For this project, we generated new structural maps and cross sections (Figs. 2–5) of three Early Cretaceous intrusions: the Malaspina pluton and Breaksea and Resolution orthogneisses. The maps and profiles reveal the three-dimensional geometry and extent of magmatic structures (Fig. 2), migmatitic granulite-facies foliations (Fig. 3), and retrograde upper-amphibolite-facies shear zones (Fig. 4). The spatial distributions

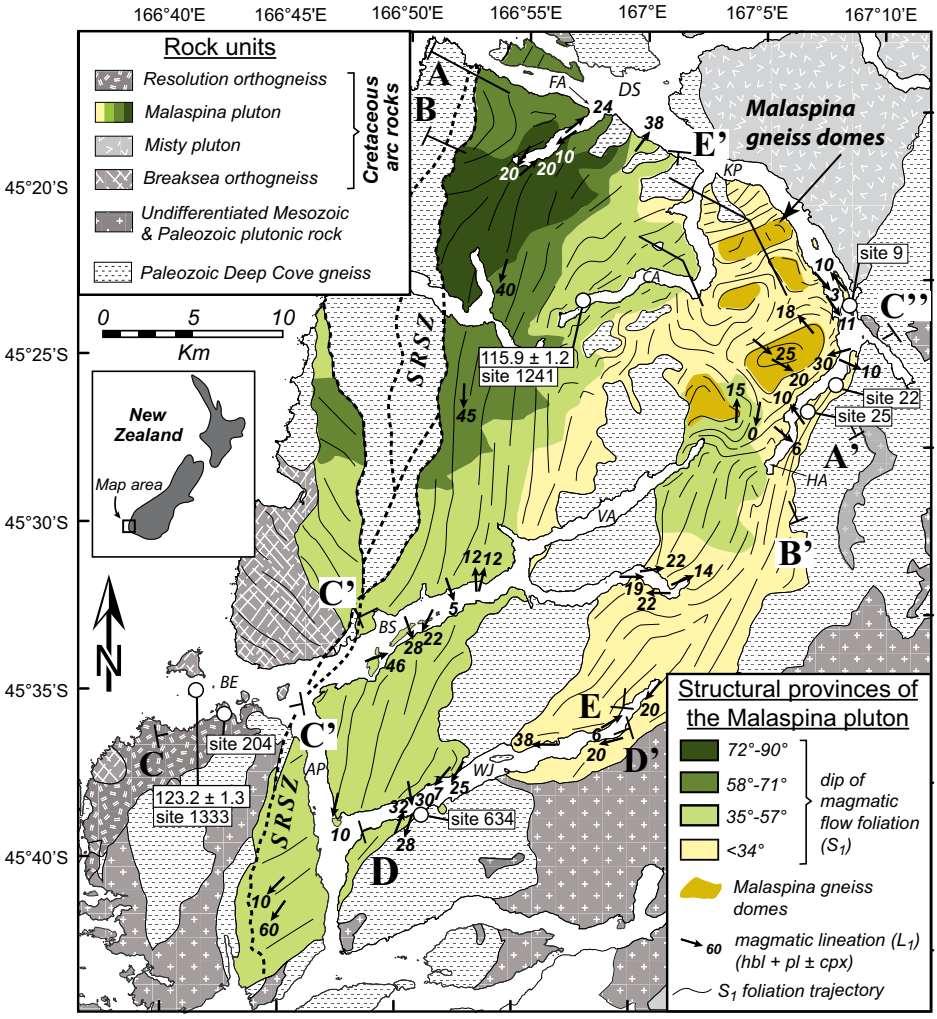

Figure 2. Map of central Fiordland showing the geometry of magmatic foliations (S_1) and lineations (L_1) in the Malaspina pluton. Foliation trajectories outline five domes of mostly metadioritic gneiss. Data points are shown in supplementary Figure S1 (see text footnote 1). Cross sections are shown in Figure 5. SRSZ—Straight River shear zone, AP—Acheron Passage, DS—Doubtful Sound, BS—Breaksea Sound, BE—Breaksea entrance, CA—Crooked Arm, FA—First Arm, HA—Hall Arm, KP—Kellard Point, VA—Vancouver Arm, WJ—Wet Jacket Arm. Sample sites and U-Pb zircon ages are indicated. Mineral abbreviations: hbl—hornblende, cpx—clinopyroxene, pl—plagioclase.

of data used to create the maps and sections are shown in supplementary Figure S1.[1]

To describe the geological history of the region, we used crosscutting relationships, U-Pb geochronology, and the distinctive characteristics of three groups of rock fabrics (L_1/S_1, L_2/S_2, and L_3/S_3) to develop a three-stage sequence of events (D_1–D_3; Fig. 6). These groupings provided a useful basis for comparing structures in different areas because the relative age of high-grade L_2/S_2 structures is bracketed by the presence of early-formed dikes and igneous layering on the low end (D_1) and by the widespread occurrence of crosscutting upper-amphibolite-facies shear zones and intraplate (A-type) felsic dikes on the high end (D_3). We also used U-Pb zircon geochronology to place age limits on each event and to facilitate structural correlations within each intrusion. These comparisons were aided by the identical crystallization ages of the Malaspina pluton and Resolution orthogneiss. Next, we provide descriptions of the structures that make up each event, including how they are distinguished in the field (Figs. 6, 7, and 8).

[1]GSA Data Repository item 2016032, data tables of zircon $^{206}Pb/^{238}U$ dates obtained using the U.S. Geological Survey–Stanford University SHRIMP-RG ion microprobe and laser-ablation–multicollector–inductively coupled plasma–mass spectrometer (LA-MC-ICP-MS) at the Arizona LaserChron Center, is available online at www.geosociety.org/pubs/ft2016.htm, or on request from editing@geosociety.org.

First Phase (D_1): Magma Emplacement

Breaksea Orthogneiss

The Breaksea orthogneiss preserves some of the oldest and deepest (>65 km) igneous structures in the Western Fiordland orthogneiss (Fig. 2). In light-colored omphacite granulite layers, igneous banding is defined by variations in the modes of garnet, omphacite, and plagioclase. In dark-colored metabasic layers, variations in garnet-pyroxene modes produce a banded appearance where large (~1 cm), irregular garnet occurs in clusters with clinopyroxene (Fig. 7A). These latter pyroxene- and garnet-rich bands are interpreted to represent cumulate layering due to a lack of chemical zoning or reactive microstructures, and the rare earth element (REE) characteristics of the garnet cores (Clarke et al., 2013; Hout et al., 2013). The layering predates emplacement of the Malaspina pluton and Resolution orthogneiss and records magma flow and cumulate processes that mark the beginning of the D_1 event at the base of the arc (Fig. 6).

Resolution Orthogneiss

Metadiorite and metagabbro of the Resolution orthogneiss are both rich in hornblende and plagioclase. Fine-grained garnet and clinopyroxene are present but less common than in the Breaksea orthogneiss. Together with the Malaspina pluton, this unit represents a major intrusion of

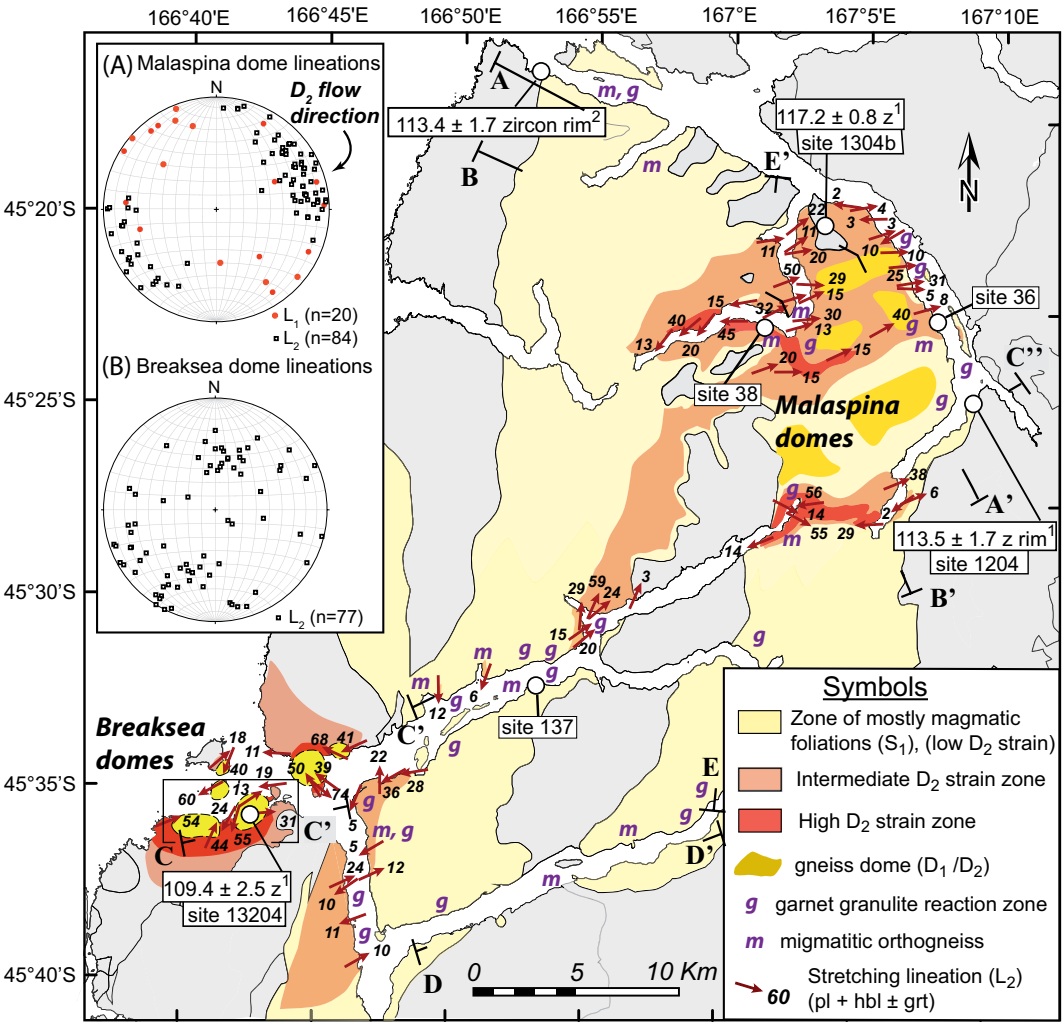

Figure 3. Map showing the geometry of migmatitic, granulite-facies foliations (S_2) and lineations (L_2) in the Malaspina pluton and parts of the Breaksea and Resolution orthogneisses. Box around Breaksea domes shows location of Figure 9. Gray shaded areas include both the Paleozoic Deep Cove gneiss and undifferentiated Mesozoic and Paleozoic plutonic rock (for more detail, refer to Fig. 2). (A–B) Lower-hemisphere equal-area stereographic projections of L_1 and L_2 mineral lineations from the Malaspina and Breaksea domes, respectively. Sample sites and U-Pb zircon ages mentioned in the text are indicated. Superscripts on ages indicate sources: 1—this study, 2—King et al. (2008). Mineral abbreviations: hbl—hornblende, grt—garnet, pl—plagioclase.

mafic-intermediate magma into the lower crust during the second half of D_1 (Fig. 6).

Most structures in the Resolution orthogneiss reflect deformation that occurred after its emplacement. Nevertheless, areas of low strain preserve some early-formed magmatic features. For example, at site 204 (Fig. 2), xenoliths of dismembered Breaksea orthogneiss up to several hundred meters in diameter occur within a weakly foliated metadioritic host (Fig. 7B). The fragments preserve remnants of old garnet-pyroxene layering that is discordant with the foliation in the host, indicating the latter is younger. Folia in the host occur as clots of aligned igneous hornblende and plagioclase that are deflected around xenoliths, indicating that the garnet-pyroxene clusters were more viscous and resisted deformation during flow. Cuspate-lobate boundaries on the xenoliths (Fig. 7B) also reflect interactions with a lower-viscosity, partially molten matrix of the Resolution orthogneiss. These structures indicate that the emplacement of the Resolution orthogneiss disrupted the Breaksea orthogneiss, which was still hot but solid enough to break and become entrained within the younger intrusion.

Malaspina Pluton

The Malaspina pluton is mostly dioritic and monzodioritic in composition with a mineral assemblage that includes plagioclase and hornblende with lesser amounts of clinopyroxene, orthopyroxene, biotite, and quartz. Two pyroxene varieties are most common in northern sectors. The main dioritic parts host a variety of dikes, sills, and xenoliths that range in composition from pyroxenite, gabbro, and hornblendite (Fig. 8A) to plagioclase-rich leucodiorite (Figs. 8B and 8C).

In areas of low D_2 strain (Fig. 3), three types of foliation (S_1) are common: (1) the preferred orientation of coarse hornblende (hbl) and clinopyroxene (cpx) within a plagioclase (pl) matrix, (2) compositional banding composed of gabbro, dioritic gneiss, and thin (1–2 cm) plagioclase-rich veins, and (3) aligned clots of mafic (hbl ± cpx) material and plagioclase aggregates inside and at the margins of ultramafic, mafic, and intermediate dikes (Figs. 8A and 8B). In areas of high D_2 strain, remnants of S_1 occur as mafic schlieren (Fig. 8E) and tightly folded mafic-ultramafic layers.

Away from D_2 shear zones, mafic-ultramafic dikes record mingling and mixing with their dioritic hosts. The oldest dikes display scalloped, nonplanar margins where S_1 folia in the host locally are truncated and deflected around apophyses (box a, Fig. 8A), indicating a contrast in effective viscosity between the two magmas. Elsewhere along the dike contact (box b, Fig. 8A), accumulations of plagioclase penetrate the dike to variable degrees, forming internal foliations that are continuous with external S_1 folia. This latter texture indicates that, at the time the foliation formed, the magmas were crystal rich and possessed similar effective viscosities

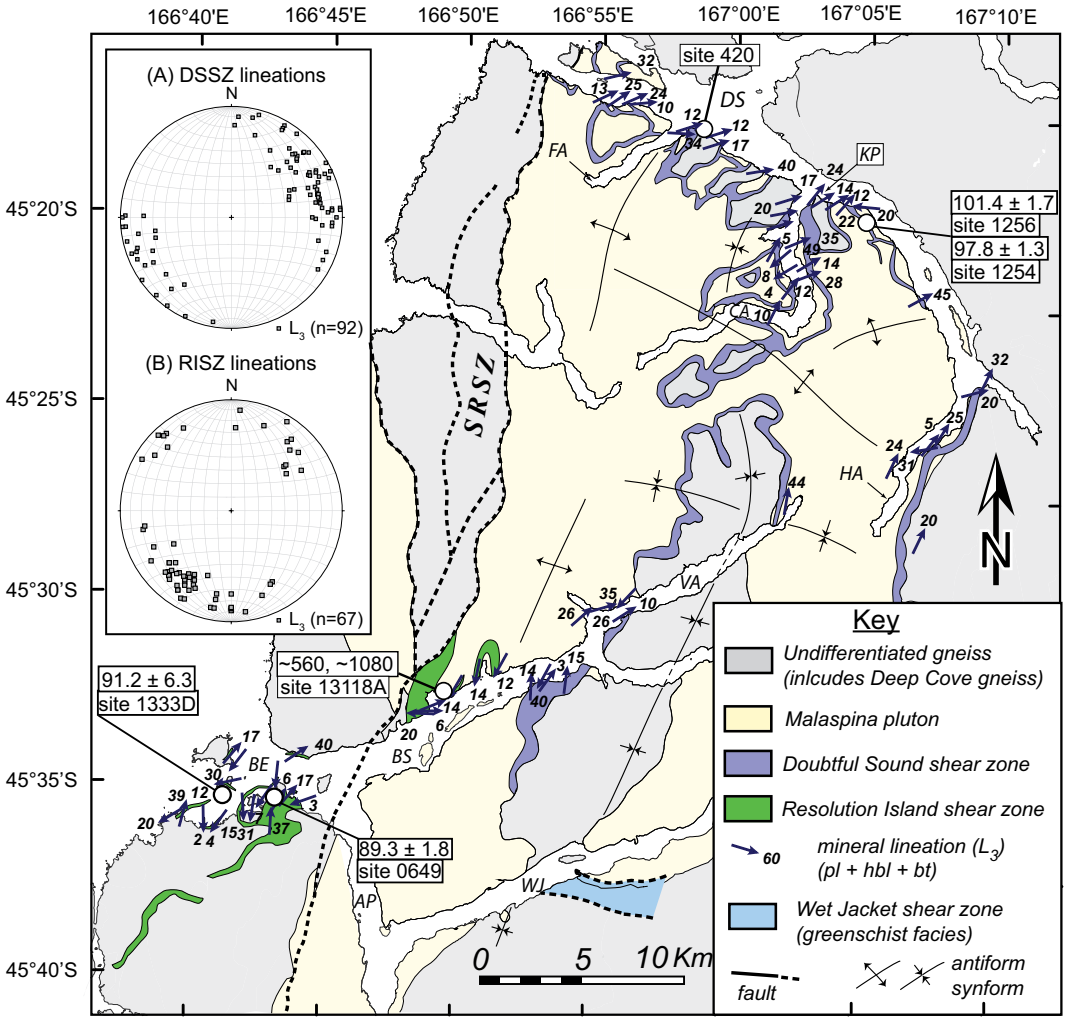

Figure 4. Map showing the geometry of retrograde, upper-amphibolite-facies foliations (S_3) and mineral stretching lineations (L_3) in the Malaspina pluton and units at Breaksea entrance. (A–B) Lower-hemisphere equal-area stereographic projections of L_3 mineral stretching lineations in the Doubtful Sound shear zone (DSSZ) and Resolution Island shear zone (RISZ), respectively. Field sites and U-Pb zircon ages are indicated. AP—Acheron Passage, DS—Doubtful Sound, FA—First Arm, HA—Hall Arm, KP—Kellard Point, BS—Breaksea Sound, BE—Breaksea entrance, VA—Vancouver Arm, WJ—Wet Jacket Arm, SRSZ—Straight River shear zone. Brittle faults are omitted for clarity. Mineral abbreviations: hbl—hornblende, bt—biotite, pl—plagioclase.

as they mingled and deformed. The variety of structures illustrates that the mafic dikes record a range of effective viscosities during hypersolidus deformation (D_1), most likely resulting from variations in grain size, composition, temperature, crystal concentration, and melt volume (Blake and Fink, 2000; Yoshinobu et al., 2009).

Felsic dikes that cut the mafic-ultramafic intrusions also record a range of viscosity contrasts and variable degrees of crystal exchange with their magmatic hosts. Figure 8B shows a leucocratic dike where internal S_1 folia defined by coarse hornblende are continuous with S_1 in a dioritic host. The dike displays slightly irregular margins where hornblende and plagioclase crystals are frozen with one end in the dike and the other in the host. Some minor refraction of S_1 occurs where it enters the dike, indicating a small contrast in effective viscosity between the magmas. This shared foliation formed late in the crystallization history of the magmas at a stage when both were viscous and crystal rich. The textures contrast with those displayed by a younger set of hornblende-bearing dikes (Fig. 8C) that truncate S_1, display no internal foliation, and exhibit planar margins.

These relationships illustrate that the dominant fabric (L_1/S_1) in the Malaspina pluton formed late in the history of the pluton, following its emplacement. The interactions exhibited by the dikes and their dioritic hosts record intrusion into an increasingly viscous, crystal-rich mush, where effective viscosity contrasts between magmas of different composition were low prior to the onset of D_2. These interactions represent the final stages of D_1, when the main body of the Malaspina pluton had mostly crystallized and solidified.

Second Phase (D_2): High-Grade Metamorphism and Migmatitic High-Strain Zones

Breaksea and Resolution Orthogneisses

At Breaksea entrance, the Breaksea orthogneiss records high-grade metamorphism that resulted in a variety of omphacite granulite assemblages in intermediate gneiss and eclogitic assemblages in mafic gneiss. Migmatite is common in the intermediate layers. In the Resolution orthogneiss, garnet-bearing metamorphic mineral assemblages and migmatite also are present but less common than in the Breaksea orthogneiss. At site 656 (Fig. 9), for example, veins of leucosome in a migmatitic part of the former unit contain large peritectic garnet crystals that overprint an older gneissic (S_2) foliation (cf. fig. 5f *in* Betka and Klepeis, 2013). The foliation is defined by the shape-preferred orientation of plagioclase and hornblende surrounding small garnet-bearing clusters. In the younger leucosome, a coarse garnet-plagioclase mineral assemblage shows only weak shape-preferred orientations, indicating the vein was emplaced after deformation began. This site illustrates that melts moved through the

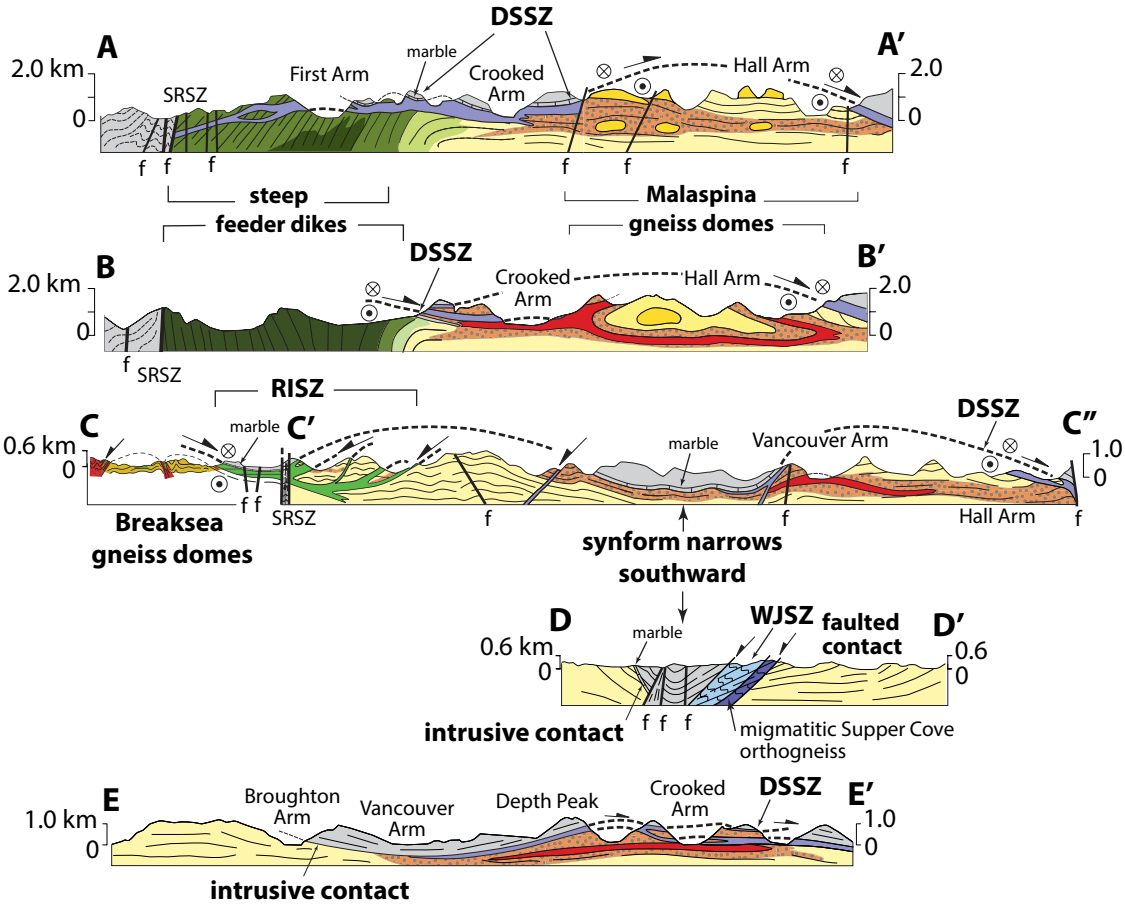

Figure 5. Cross sections showing the geometry of foliations, faults, and shear zones in the Malaspina pluton and adjacent units (locations shown in Figs. 2 and 3). In C, the section C–C′ is raised 375 m relative to section C′–C″ to account for the effects of late faulting and to match structures across Breaksea entrance. SRSZ—Straight River shear zone, f—fault, DSSZ—Doubtful Sound shear zone, RISZ—Resolution Island shear zone, WJSZ—Wet Jacket shear zone.

section in the form of veins, patchy leucosome, and dikes (Fig. 7D) that intruded high-strain zones during and after deformation. We group this activity into a second event (D_2) that occurred after emplacement of the Resolution orthogneiss (Fig. 6).

Areas of low strain within both the Breaksea and Resolution orthogneisses preserve delicate migmatitic and metamorphic textures that generally are absent in high-strain zones. These include xenoliths that preserve old igneous layering inside them within the Resolution orthogneiss (site 204, Fig. 7B). Similar textures occur in a low-strain zone at site 197 (Fig. 7C), which shows a disaggregating layer of garnet-pyroxenite in the Breaksea orthogneiss. Fractures filled with plagioclase-rich material derived from the matrix indicate that this mafic layer broke apart within a partially molten host. Some fractures show sigmoidal and wedge-shaped geometries that terminate inside the clusters, suggesting they initiated at their boundaries and propagated inward. Others penetrate through the clusters and record the early stages of boudinage. Both sites exhibit weakly deformed, fine-grained garnet that is concentrated along the boundaries between mafic pieces and an enclosing plagioclase-rich matrix. Similar features are either absent or deformed in high-strain zones, indicating that the metamorphism occurred either prior to or during D_2.

Areas of high strain are characterized by the appearance of a penetrative S_2 foliation that cuts and transposes all igneous layering in both the Breaksea and Resolution orthogneisses. Mineral lineations (L_2), defined by aligned aggregates of plagioclase, pyroxene, and/or hornblende, are ubiquitous. Linear fabrics (L > S and L = S) are dominant. Migmatite in these zones shows large (1–2 cm) pressure shadows of plagioclase-rich material around mafic clusters (Fig. 7E). Potassium feldspar (ksp) and quartz (q) also are present. The occurrence of asymmetric shear bands, fractured garnet-omphacite clusters filled with leucosome (Fig. 7E), pyroxene fish, and tight folds of dikes (Fig. 7D) indicates high strains. These S_2 foliations form approximately concentric trajectories that define the Breaksea gneiss domes (Fig. 9; Betka and Klepeis, 2013).

In one well-preserved example of a high-strain zone on Hāwea Island (Fig. 9), pockets of weakly deformed migmatite occur in a strain shadow around a block of garnet pyroxenite (Figs. 7F and 7G). Outside the strain shadow, S_2 folia wrap the block, forming a high-strain zone and illustrating that the block resisted deformation during flow. This site preserves three textural zones that record the transition from low to high strain in a rock that was once partially molten. The strain gradations are expressed as low-strain zone 1, intermediate-strain zone 2, and high-strain zone 3.

Low-strain zone 1. Low-strain zone 1 (Fig. 7G) occurs inside the strain shadow and shows plagioclase-rich leucosome (pl + ksp + q) surrounding poorly aligned clusters of coarse (up to 1 cm) garnet and omphacite. The clusters are similar to those that make up cumulate layering inside the block of mafic gneiss and are interpreted to reflect the same igneous origin. However, unlike the layering inside the block, the clusters in the strain shadow display fractures filled with leucosome. The leucosome forms angular shapes with many branching apophyses that are absent in the other two textural zones. Plagioclase is coarse and shows little evidence of grain-size reduction by crystal-plastic deformation mechanisms.

Intermediate-strain zone 2. Intermediate-strain zone 2 includes migmatitic gneiss at the edge of the strain shadow. This area shows the

Unit	Event	Structures	Orientations	Textures	Metamorphism	*P-T* history	Age
Malaspina Orthogneiss	D_3	S_3 Medium to fine, locally mylonitic & gneissic foliations with hbl, bt, cz	gently dipping to N, NNE & NNW, including DSSZ	Planar (S > L) and linear (L = S) fabrics common, top-down-to-NE & -NNE shear sense (down-dip) most common	Retrogression to upper amphibolite facies assemblages (hbl, cz, bt, pl, q after gnt, cpx)	Decompression with cooling to P ≈ 0.7-0.9 GPa, T ≈ 550-650°C[1]	Deformation and metamorphism at 106-98 Ma
		L_3 Mineral stretching lineations with aligned hbl, bt, pl, cz	Gently-mod. plunging, most trend to NNE, NE				
	D_2	S_2 Migmatitic, gneissic foliations with gnt, cpx and hbl clusters in pl matrix	Gently dipping high-strain zones wrapping gneiss domes in NE sector	Linear fabrics (L > S and L = S) dominant, both top-to-NE and top-to-SW shear senses occur in flat migmatitic high-strain zones	Multiple pulses of garnet granulite facies metamorphism & partial melting, recrystallization of S_1 mineral assemblages	P ≈ 1.2-1.45 GPa T ≈ 850-900°C at either constant pressure or subtle loading[3]	Deformation at 114-106 Ma, partial melting and garnet granulite metamorphism at 116-111 Ma
		L_2 Mineral stretching lineations with aligned pl, cpx, gnt	Gently plunging, most trend to ENE-WSW				
	D_1	S_1 Magmatic foliations in hbl diorite with mafic minerals hbl, cpx, ± opx ± bt ±cz	Subvertical dips in NW sector, concentric with gentle dips, forming domes to SE	Planar (S > L) fabrics most common, mafic-interm. dikes record variable degrees of comagmatic exchange with crystal-rich dioritic hosts	Emplacement accompanied by garnet granulite metamorphism and localized partial melting in host rock		Initial diking by ~120 Ma, most at 118-115 Ma
		L_1 Mineral lineations with aligned hbl, pl, and cpx	Most trend to NW-SE in NE sector, elsewhere to NE-SW				
Breaksea & Resolution orthogneisses	D_3	S_3 Medium to fine, locally mylonitic & gneissic foliations with hbl, bt, cz	curved, wrapping gneiss domes, including RISZ	Planar (S > L) and linear (L = S) fabrics common, top-to-NE & -NNE shear sense (down-dip & strike-slip) most common	Retrogression to upper amphibolite facies assemblages (hbl, cz, bt, pl, q after gnt, pyroxene)	Decompression with cooling to P ≈ 0.9-1.4 GPa, T ≈ 650-750°C[2]	Deformation and metamorphism at 95-89 Ma
		L_3 Mineral stretching lineations with aligned hbl, bt, pl, cz	Gently-moderately plunging, most trend to NNE, NE or NW				
	D_2	S_2 Migmatitic, gneissic foliations with clusters of hbl or gnt, om	Concentric gneiss domes separated by curved steep high strain zones	Linear fabrics (L > S and L = S) dominant, dome-side-up shear senses occur in steep migmatitic high-strain zones	Omphacite granulite and eclogitic facies metamorphism (BO), partial melting, recrystallization of S_1 mineral assemblages	Near-isothermal decompression from P ≈ 1.8 GPa to P ≈ 1.4 GPa at T ≈ 850°C[2]	Deformation, partial melting and high-grade metamorphism at 114-95 Ma
		L_2 Mineral stretching lineations with aligned pl and either om or hbl	Radial patterns around domes, steep plunges in steep shear zones				
Resolution Orthogneiss	D_1	S_1 Coarse-medium, gneissic foliations defined by igneous hbl, pl	Deformed into gneiss domes with S_2	S_1 deflected around xenoliths of BO			Coincided with emplacement at ~115 Ma
Breaksea Orthogneiss	D_1	S_1 Igneous bands of alternating metagabbro and metadiorite	Deformed into gneiss domes with S_2	Variations in gnt, om, pl and gnt, om modes characterize layering		P ≥ 2.0 GPa, T ≥ 900°C[2]	Coincided with emplacement at ~123 Ma

Figure 6. Table showing the chronology of geologic features in the three main plutonic units in the study area. BO—Breaksea orthogneiss, DSSZ—Doubtful Sound shear zone, RISZ—Resolution Island shear zone. Sources of pressure-temperature (*P-T*) data denoted with superscripts: 1—Klepeis et al. (2007); 2—De Paoli et al. (2009); 3—Stowell et al. (2014). Age ranges and other relationships are discussed in the text. Mineral abbreviations: hbl—hornblende, bt—biotite, gnt—garnet, pl—plagioclase, q—quartz, om—omphacite, opx—orthopyroxene, cpx—clinopyroxene, cz—clinozoisite. Mineral abbreviations are from Kretz (1983).

progressive development of a spaced S_2 foliation defined by the alignment of mafic clusters with tapered pressure shadows composed of plagioclase-rich leucosome. Plagioclase is partially recrystallized and shows smaller grain sizes than in zone 1.

High-strain zone 3. S_2 becomes increasing penetrative in high-strain zone 3, where it is characterized by partially to completely recrystallized plagioclase ribbons and stretched garnet-pyroxene clusters. The ribbons record an increase in stretching and form penetrative mineral lineations (L_2) on S_2 foliation planes. High strains are indicated by increases in the lengths of pressure shadows and in the aspect ratios of mafic clusters, and decreases in the spacing of S_2 and in plagioclase grain sizes.

These three zones illustrate the importance of crystal-plastic deformation mechanisms during D_2 as melts migrated through or crystallized within the deep root of this arc. All three exhibit fine-grained garnet surrounded by thin moats of clinopyroxene that overprint both the older garnet-pyroxene clusters and the leucosome. The secondary garnet is undeformed in zone 1 and becomes progressively more deformed in zones 2 and 3, respectively, also reflecting an increase in strain. Thus, these zones record metamorphism and deformation at the granulite facies that accompanied and postdated partial melting during the D_2 event.

Malaspina Pluton

The Malaspina pluton records pulses of granulite-facies metamorphism that resulted in partial melting and the recrystallization of older S_1 mineral assemblages, including plagioclase, hornblende, orthopyroxene, biotite, and quartz. These events resulted in the growth of three textural

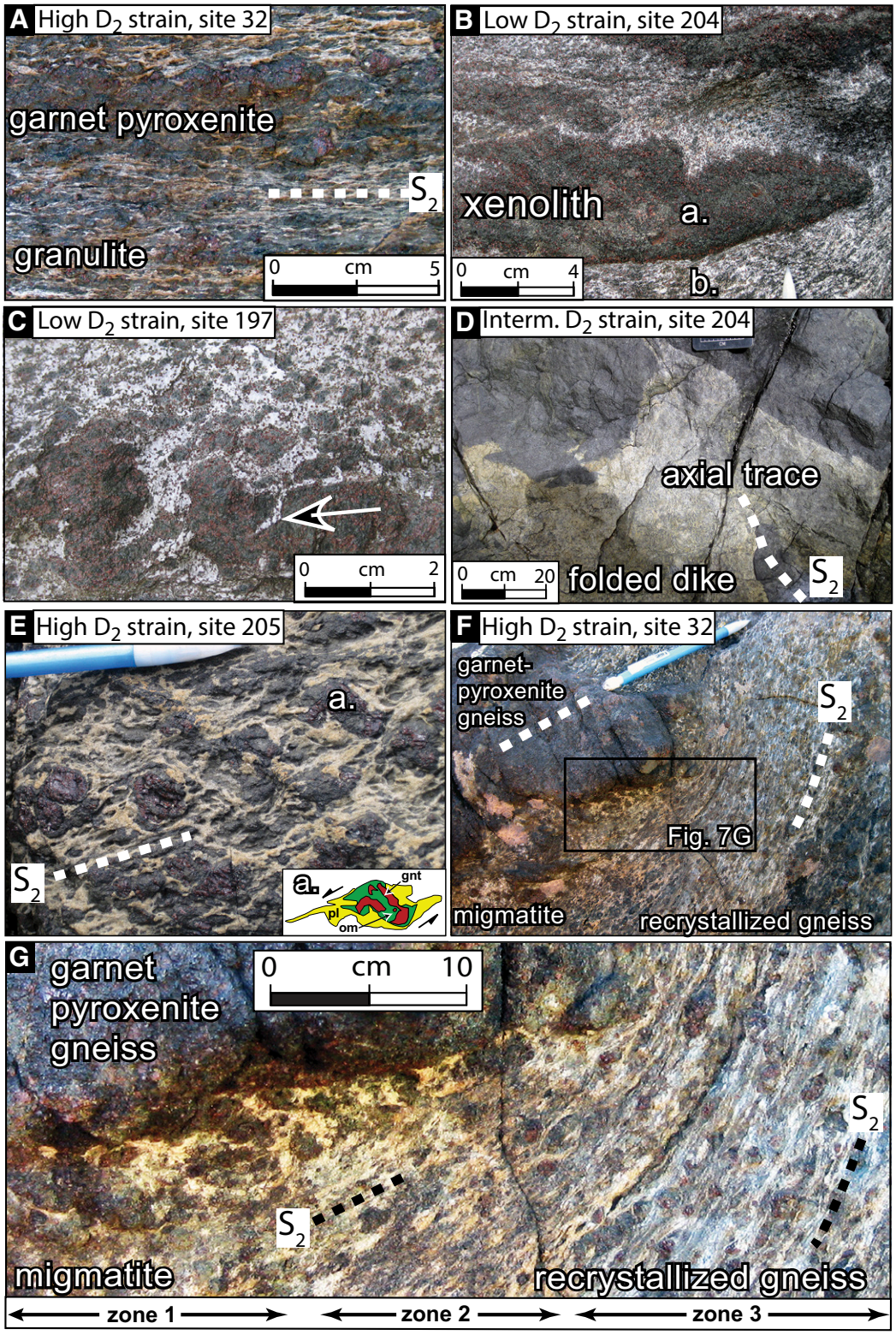

Figure 7. Photographs illustrating structures formed during D_1 and D_2 within the Breaksea and Resolution orthogneisses (locations shown in Figures 2, 9). (A) Garnet pyroxenite interlayered with omphacite granulite in the Breaksea orthogneiss. (B) Xenoliths of garnet pyroxenite (a.) showing preferred orientations in a foliated metadioritic host (b.) in the Resolution orthogneiss. (C) Garnet pyroxenite layer disaggregating in a migmatitic host (Breaksea orthogneiss). Arrow points to a fracture filled with plagioclase-rich material derived from the host. (D) Leucocratic dike cuts S_2 in a high-strain zone and is also folded within it. Dike yielded a 109.4 ± 2.5 Ma U-Pb zircon crystallization age (sample 13204). (E) Pressure shadows of plagioclase-rich material surround mafic (gnt + cpx) clusters in migmatitic high-strain zone (D_2). Inset shows detail of clast labeled a. Mineral abbreviations: cpx—clinopyroxene, gnt—garnet, pl—plagioclase, om—omphacite. (F) Block of mafic gneiss wrapped by external S_2 folia in a high-strain zone in the Breaksea orthogneiss. (G) Detail of area outlined by box in Figure 7F.

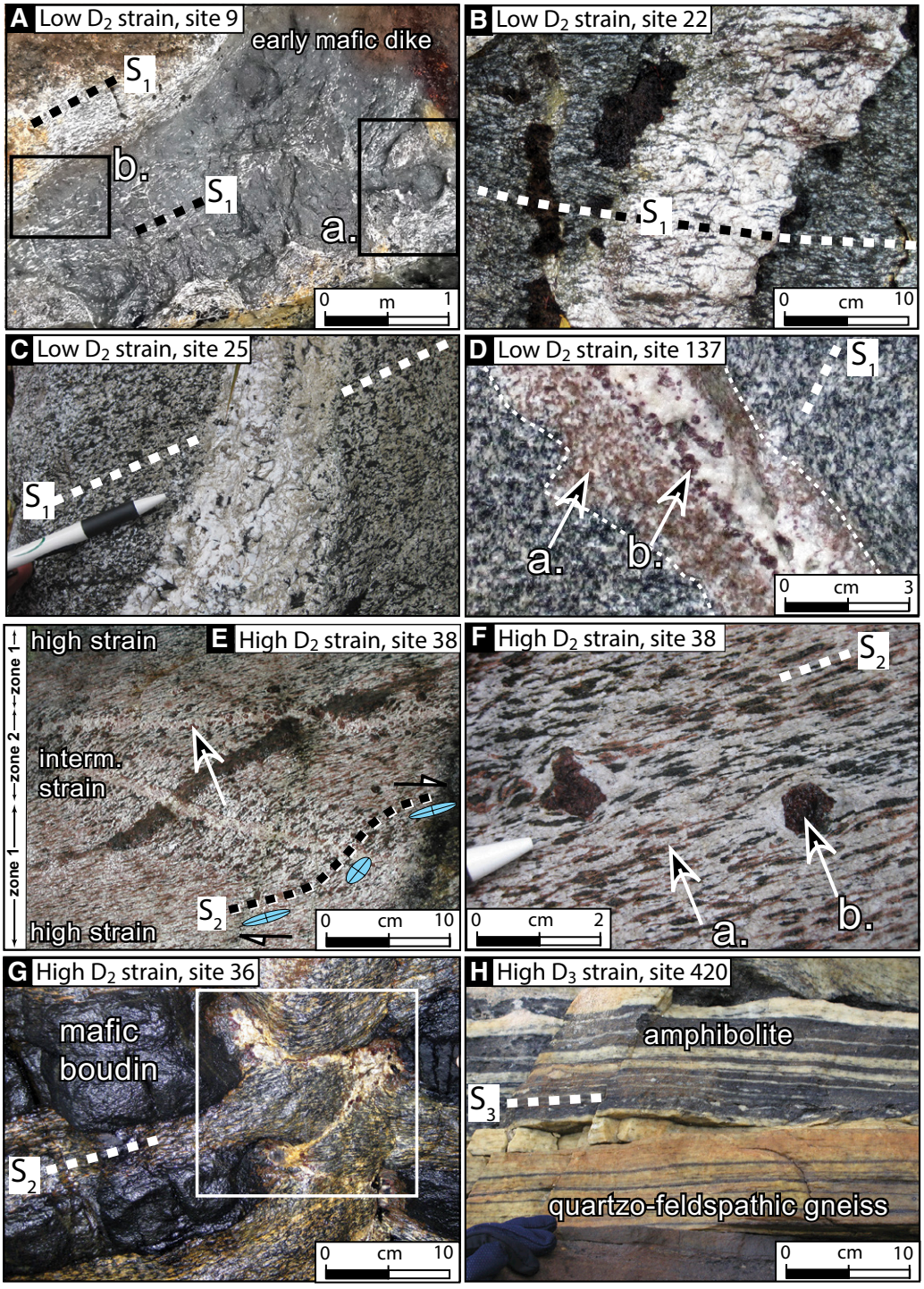

Figure 8. Photographs illustrating structures formed during D_1, D_2, and D_3 within the Malaspina pluton (site locations shown in Figs. 2, 3, and 4). (A) Hornblendite dike hosted by dioritic gneiss. S_1 in host is truncated and deflected around dike apophyses (box a.). Plagioclase crystals penetrate the dike to variable degrees, forming internal flow foliations that are continuous with external S_1 folia (box b.). (B) Leucocratic dike showing an internal S_1 foliation defined by aligned hornblende that is continuous with S_1 in dioritic host. (C) Late hornblende-bearing dike that truncates S_1 and displays no internal foliation. (D) Leucosome vein in low-strain migmatitic gneiss bordered by a garnet granulite reaction zone (a.—type 1 garnet; b.—type 2 garnet). (E) Migmatitic gneiss in a high-strain zone showing mafic schlieren and a penetrative S_2 foliation. Zone 1 exhibits highest strains and is characterized by fine-grained recrystallized plagioclase in mylonite. Zone 2 exhibits intermediate strains and is characterized by coarse plagioclase. Changes in foliation orientation in the two zones, and asymmetric schlieren, give a top-to-the-SW (right) shear sense. Leucosome vein (arrow) with type 2 garnet cuts mylonite. (F) Mylonitic gneiss in a high-strain area (zone 1) shows type 1 (a.) and type 3 (b.) garnet. Type 1 garnet and clinopyroxene form coronas around hornblende. Type 3 shows plagioclase-rich pressure shadows. (G) Leucosome with type 3 garnet in boudin necks. (H) High-strain zone (D_3) within the Doubtful Sound shear zone showing recrystallized quartzofeldspathic gneiss interlayered with mylonitic amphibolite containing plagioclase augen in the Deep Cove gneiss.

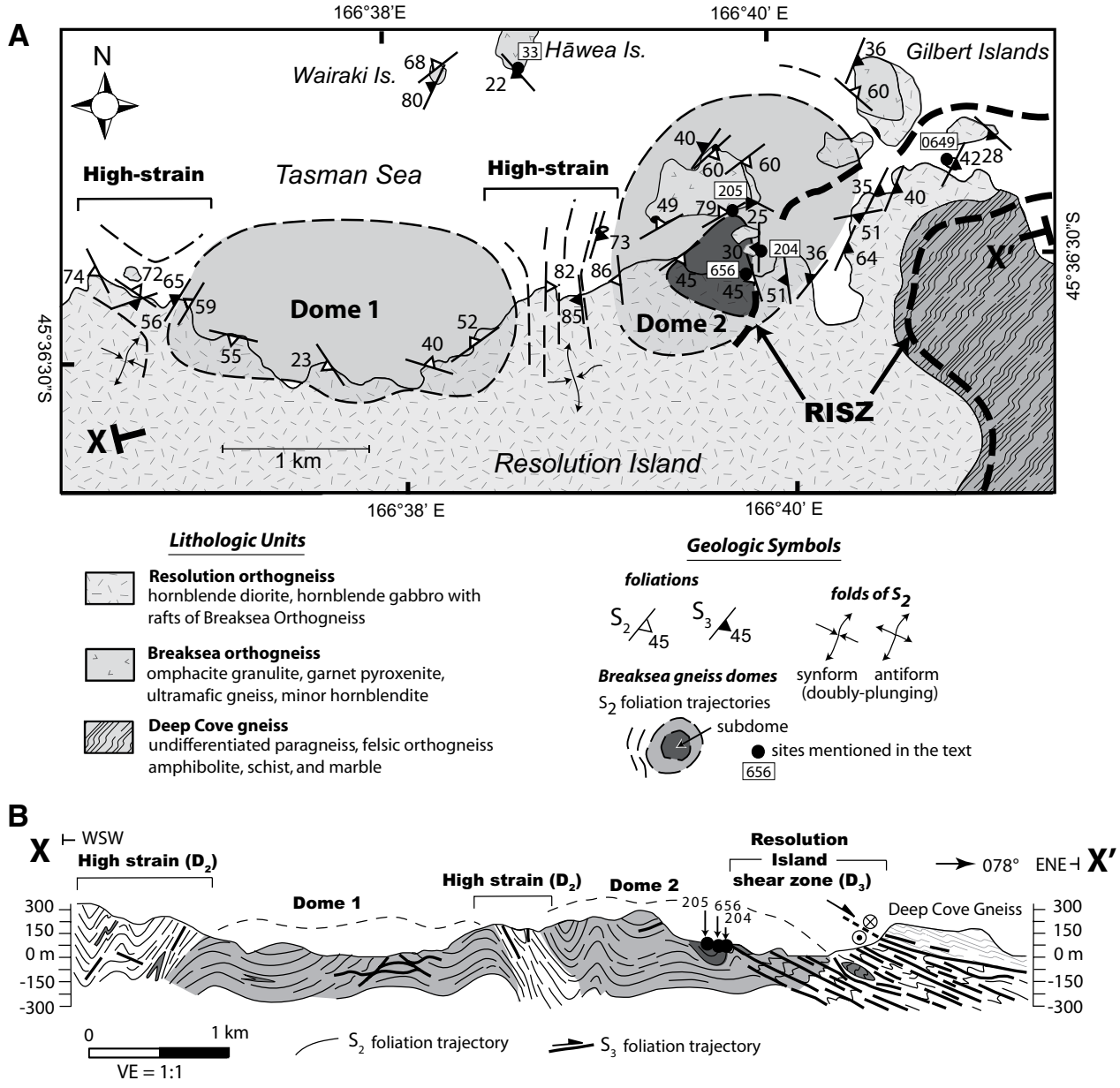

Figure 9. (A) Map and (B) cross section of the Breaksea domes (modified from Betka and Klepeis, 2013; locations in Fig. 3). Shading of Resolution orthogneiss in B is omitted for clarity. Thin black lines are S_2 foliation trajectories that define the domes. Numbers refer to sites discussed in the text. RISZ—Resolution Island shear zone. VE—vertical exaggeration.

types of garnet that occur within all sectors of the pluton. The first two types are associated with plagioclase-rich veins of leucosome, some of which are bordered by narrow (1–2 cm) garnet granulite reaction zones (Fig. 8D). Type 1 garnet is fine grained and intergrown with clinopyroxene in these reaction zones (a, Fig. 8D). Type 2 garnet occurs as coarse porphyroblasts inside the veins (b, Fig. 8D). Type 3 occurs as porphyroblasts surrounded by plagioclase-rich haloes without veins (Fig. 8F). Previous work (Oliver, 1977; Clarke et al., 2005; Allibone et al., 2009a; Stowell et al., 2014) has linked the growth of type 2 and 3 garnet, and the veins and haloes, to in situ partial melting during metamorphism. Type 1 garnet appears to be a product of dehydration as melt in veins absorbed water from the surrounding rock (Daczko et al., 2001; Clarke et al., 2005). We grouped all of these features into the second tectonic event (D_2), which began after emplacement of the Malaspina pluton (Fig. 6). We used their widespread occurrence and variable degrees of deformation to map areas of high, intermediate, and low D_2 strain within the pluton (Fig. 3).

Deformation that was synchronous with partial melting and granulite-facies metamorphism resulted in two main zones of high to intermediate strain in the NE and SW quadrants of the pluton (Fig. 3). All other areas constitute low-strain zones. In low-strain areas, S_1 igneous assemblages are dominant, and leucosome in migmatite is patchy and undeformed. Veins with garnet granulite reaction zones typically cut S_1 at variable angles and display sharp, planar boundaries (Fig. 8D).

Plagioclase aggregates are coarse to medium grained and are not extensively recrystallized. In these same areas, type 3 garnet exhibits haloes of plagioclase-rich material that are either undeformed or show weak pressure shadows.

High- and intermediate-strain zones are characterized by the appearance of penetrative S_2 folia that cut and transpose all S_1 foliations. Folia of S_2 are defined by stretched aggregates of recrystallized plagioclase and deformed clusters of garnet, clinopyroxene, and hornblende (Figs. 8E and 8F). In migmatite, haloes of plagioclase-rich leucosome form large (1–2 cm) pressure shadows around coarse garnet (type 3) porphyroblasts (Fig. 8F). Mineral stretching lineations (L_2), composed of plagioclase and garnet-clinopyroxene aggregates, form penetrative L > S and L = S fabrics. Zones of the highest strain (Fig. 3) are distinguished by the presence of mylonite, where plagioclase forms long (1–2 cm) recrystallized ribbons that show a reduction in grain size compared to intermediate-strain areas (Fig. 8E). This grain-size reduction was achieved by crystal-plastic deformation mechanisms, including dislocation creep (cf. Klepeis et al., 2007). The occurrence of asymmetric shear bands, pyroxene fish, tight folds of dikes, asymmetric schlieren (Fig. 8E), and boudinaged mafic layers (Fig. 8G) also indicates high strains.

The synchronicity of partial melting, granulite-facies metamorphism, and D_2 deformation is indicated by zones of migmatite that were recrystallized to mylonite, and then cut by younger veins and patches of garnet-bearing (types 1, 2, and 3) leucosome (Fig. 8E). Type 3 garnet that overprints mylonitic S_2 foliation also exhibits haloes of plagioclase-rich material interpreted to represent former melt (Fig. 8F). Clots of leucosome with type 2 (peritectic) garnet in them collected in boudin necks enveloped by mylonitic gneiss (Fig. 8G), indicating that melts had migrated into dilational sites during deformation. These textures show that D_2 was characterized by episodes of partial melting and high-grade metamorphism and that deformation facilitated the mobilization of partial melts within the crust.

Third Phase (D_3): Upper-Amphibolite-Facies High-Strain Zones

Deformation (D_3) accompanying retrograde upper-amphibolite-facies metamorphism resulted in shear zones that cut all L_2/S_2 fabrics. All of these shear zones display gneissic and locally mylonitic foliations (S_3) composed of hornblende, clinozoisite, biotite, plagioclase, and quartz (Fig. 8H). Where strains are moderate, such as the margins of shear zones and in strain shadows around mafic pods, hornblende and clinozoisite form asymmetric fringes around cores of S_2 garnet and pyroxene. In mylonites, garnet and pyroxene are rare, suggesting these phases reacted out during retrograde metamorphism. Biotite beards on plagioclase and hornblende, and increased modes of hornblende and biotite suggest high fluid activities.

In areas of low D_3 strain, S_3 typically is weak and defined by aligned intergrowths of hornblende and fine-grained plagioclase. Biotite is commonly clustered rather than forming a penetrative S_3 foliation. In contrast, high-strain zones exhibit increased mineral alignment, decreased spacing of S_3 folia, and a reduction in plagioclase and quartz grain sizes compared to low-strain areas. High-strain zones also show penetrative hornblende and plagioclase mineral stretching lineations (L_3), asymmetric shear bands, and asymmetric hornblende and clinozoisite fish. Both top-down-to-the-NE and -SW senses of shear are common, with the former dominating (cf. Klepeis et al., 2007). On the basis of similarities in metamorphic grade, structural style, and age relative to D_2 structures, we grouped all of these shear zones into the D_3 event (Fig. 6). Nevertheless, as we show later, these structures form two distinctive systems that record a spatial and temporal migration of deformation from NE to SW across the field area.

Late Faults and Shear Zones

Superimposed on all upper-amphibolite-facies shear zones are sets of brittle faults and greenschist-facies shear zones. The latter group includes the Straight River shear zone (Fig. 2), which deforms the western margin of the Malaspina pluton (King et al., 2008), and the Wet Jacket shear zone (Figs. 4 and 5D), which deforms its eastern margin. The low metamorphic grade of these two structures, and their association with brittle faults of probable Tertiary age, suggests they formed late in the history of the region. The brittle faults include both strike-slip and normal populations. Displacements range from a few centimeters to approximately a kilometer. All of these features are easily distinguished from older Cretaceous structures.

THREE-DIMENSIONAL GEOMETRY OF STRUCTURES

Igneous Structures

The trajectories of S_1 foliations (Fig. 2) reveal the internal structure of the Malaspina pluton. In its NW quadrant, subvertical (72°–90°) magmatic foliations (S_1) define a 6-km-wide zone that gradually flattens to the E and SE, where 1–2-km-thick sills dip less than 34° (Figs. 2, 5, and 10). In western regions, where S_1 is steepest (green areas of Fig. 2), hornblende and plagioclase mineral lineations (L_1) are moderately to gently plunging and mostly trend N-S and NE-SW. In eastern regions, where S_1 is shallowest (yellow areas of Fig. 2), the lineations mostly trend E-W and SE-NW. South of First Arm (Fig. 2), S_1 twists smoothly into a zone of moderately dipping (35°–57°) foliations, defining a mushroom-shaped igneous body. The steep orientations of dikes on its NW and W sides suggest the ascent of magma out of this zone and into the areas of gently dipping sills to the S and E, where magma ponded below a roof of Deep Cove gneiss.

Intrusive Contacts and Thermal Aureoles

Intrusive contacts between the Malaspina pluton and the Deep Cove gneiss, and thermal aureoles within the latter, record processes that accompanied lower-crustal magmatism. One of the best-preserved contacts occurs at the western end of Wet Jacket Arm, where the Malaspina is a coarse-grained hornblende-pyroxene diorite with a weak S_1 foliation (Fig. 2). Steep garnet granulite reaction zones cut the foliation and are undeformed, indicating low strains. At the contact (site 634, Fig. 2), the boundary is sharp (<1 m) and dips steeply to the ESE. It also is folded by an upright NNE-trending synform that lacks an axial planar cleavage and, locally, is steepened by late faults (Fig. 5D). These latter structures indicate that the steep orientation most likely reflects deformation at low metamorphic grade that occurred after pluton intrusion.

The Deep Cove gneiss at Wet Jacket Arm is composed of thick (2 m) marbles and calcareous schist interlayered with metapsammite, garnet-biotite gneiss, and amphibolite. A gneissic foliation defined by aligned biotite, hornblende, quartz, plagioclase, and garnet is discordant with S_1 in the Malaspina pluton. Hornfels and migmatite occur up to 1 km east of the contact. Veins of leucosome are unfoliated and display irregular shapes that disrupt older gneissic foliations in the host rock, indicating that the migmatite has not been penetratively deformed. Misaligned hornblende and biotite overgrowths on garnet and feldspar porphyroblasts suggest a history of amphibolite-facies metamorphism accompanying pluton emplacement (cf. Chavez et al., 2007; Allibone et al., 2009a; Daczko et al., 2009). These relationships indicate that deformation was partitioned within the pluton during both D_1 and D_2, leaving the host rock mostly undeformed.

Elsewhere in the study area, migmatite occurs in contact aureoles that range in thickness from 0.2 to 1 km at the eastern end of Wet Jacket Arm,

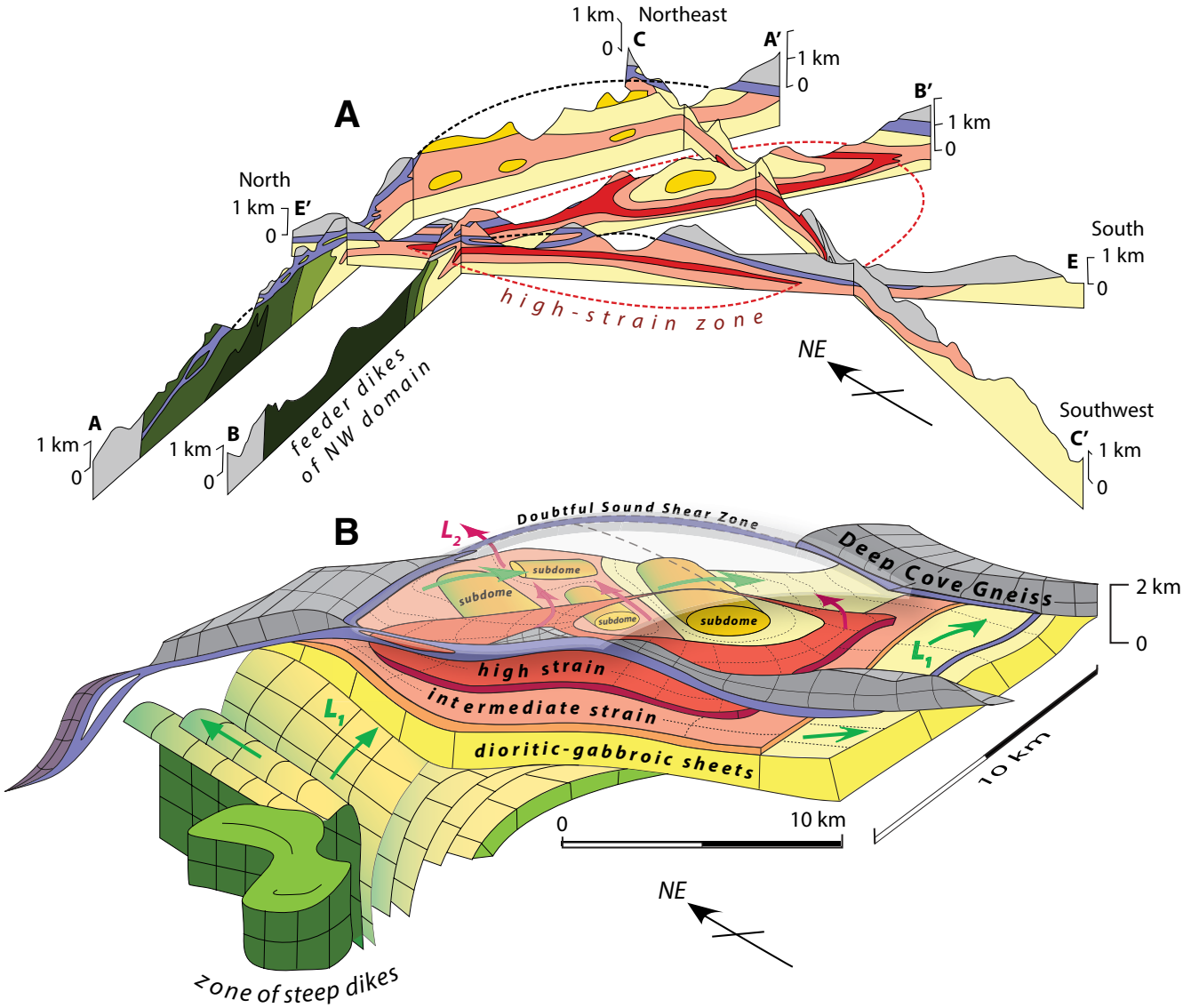

Figure 10. (A) Composite cross-sectional fence diagram showing geometry of structures in the NE Malaspina pluton. View is to the east. (B) Isometric block diagram emphasizing the three-dimensional geometry of the Malaspina gneiss domes. Fence diagram in A was constructed using cross sections shown in Figure 5; block in B was constructed from A.

in Acheron Passage, at the western and eastern ends of Breaksea Sound, at the northern end of Hall Arm (site 1204A, Fig. 3), along the western reaches of Doubtful Sound, and above the Doubtful Sound shear zone at Kellard Point (Fig. 4; cf. Allibone et al., 2009b). Some of these localities are deformed by D_3 shear zones (Fig. 4). The widespread occurrence of migmatite in narrow aureoles, and their general absence elsewhere in the Deep Cove gneiss, suggests they formed during and shortly after emplacement of the Malaspina pluton, either by in situ partial melting and/or by the injection of igneous material.

Intrusive contacts between the Malaspina pluton and Breaksea orthogneiss do not appear to have survived in most areas. Allibone et al. (2009a) described rare dikes of garnet-pyroxene diorite similar to the Malaspina that intruded the Breaksea orthogneiss west of the Straight River shear zone. We observed xenoliths of garnet-omphacite pyroxenite within the Malaspina intrusion along the eastern side of Acheron Passage (AP, Fig. 2). The compositions and textures of these xenoliths are similar to rocks in the Breaksea orthogneiss. We therefore interpret them to be rafts of the latter that were entrained in the Malaspina pluton during emplacement.

East of the zone of steep and moderately dipping dikes, and near the roof of the Malaspina pluton (site 1241, Fig. 2), sheets of metadiorite are interlayered with rafts of metasedimentary rock of the Deep Cove gneiss. Most of these rafts are aligned parallel to the margins of metadiorite sheets. Despite some local truncation of foliation planes, examples of rotated rafts are rare. This interlayering suggests that the flat parts of the intrusion were constructed by magmatic wedging during the incremental emplacement of magmatic sheets into the Paleozoic host rock.

Malaspina Gneiss Domes

In the NE sector of the Malaspina pluton, S_1 foliation trajectories reveal the three-dimensional shapes of at least five kilometer-scale domes composed mostly of metadioritic orthogneiss with minor hornblendite and

small mafic-intermediate dikes (Fig. 2). These five domes occur within a larger domed structure, ~10 km wide, between Hall Arm and Crooked Arm (Figs. 5A and 10). At the top, northern, and eastern ends of the large dome, all S_1 foliations are truncated by the Doubtful Sound shear zone. The dome's western and southern sides coincide with two areas where flat (<34°) S_1 foliation planes steepen to 35°–57° (Figs. 2 and 10). The former area continues to steepen farther west and merges into the steep igneous foliations of the NW Malaspina pluton. Foliations in the latter area flatten back to dips of less than 30° at Wet Jacket Arm.

All five gneiss domes are triaxial with flat profiles and long axes (Figs. 2 and 5). Two preferred orientations are evident. One of three northern domes is oriented parallel to the NE-SW trend of L_1 mineral lineations in the domain. The southernmost dome appears roughly equant in map view. The other three have long axes aligned parallel to the NE-SW trend of L_2 stretching lineations, which are easily distinguished from L_1 in this area on the basis of both mineral assemblage and orientation (cf. Figs. 2 and 3).

Migmatite and garnet granulite reaction zones that formed during D_2 occur within all sectors of the Malaspina pluton, including inside each of the five domes (g, m, Fig. 3). Thus, not all zones of migmatite and high-grade metamorphism coincide with areas of intermediate and high D_2 strain (Fig. 3). A 1–2-km-thick shear zone with 0.5-km-thick bands of mylonitic granulite and migmatitic gneiss forms the base and wraps around the sides of the domes (Figs. 3, 5, and 10A). Inside the shear zone, leucosome in migmatitic gneiss cuts across mylonite and also is deformed within it, indicating that the deformation involved the flow of partially molten crust (Figs. 8E, 8F, and 8G). Between the high-strain zones, a 5-km-wide region of low strain exposes the interior of the domes. These areas are composed of undeformed migmatite and patchy garnet granulite superimposed on the older (L_1/S_1) igneous fabric. This partitioning of D_2 strain around the edges of the domes suggests that these structures were relatively viscous and resisted deformation.

Mineral stretching lineations (L_2) trend to the NE and SW (Fig. 3A) and retain their gentle plunges despite the steepening of S_2 at dome margins. This pattern indicates that flow in high-strain zones was mostly horizontal. Some scatter (Fig. 3A) reflects the deflection of material around the domes during flow and some later warping. Sense-of-shear indicators, including pyroxene fish, shear bands, asymmetric mafic schlieren, deflected dikes, and oblique foliations, show predominantly top-to-the-W and -SW displacements within gently dipping S_2 shear planes exposed at Crooked Arm and Hall Arm. These areas (Fig. 3) represent the NW and SE flanks of the gneiss domes, respectively, and are closer to dome tops than bottoms (Fig. 5B). Top-to-the-E and -NE displacements also occur but are less abundant.

Breaksea Gneiss Domes

At Breaksea entrance, nearly concentric trajectories of S_2 foliation planes define several kilometer-scale domes in both the Breaksea and Resolution orthogneisses (Figs. 3 and 9A). These domes, which are described in detail by Betka and Klepeis (2013), lie beneath a carapace of Deep Cove gneiss and are separated from one another by steeply and moderately dipping migmatitic high-strain zones. The internal regions display mostly gently dipping, gently folded, locally migmatitic gneissic foliations (Fig. 9). Doubly plunging antiforms and synforms of S_2 are common in both high- and low-strain areas but are much tighter in the former (Fig. 9B). Many exhibit second-order subdomes that range in size from tens to a few hundred meters in diameter. Most are ovoid shaped and lack the flat profiles and preferred orientations of the Malaspina domes. The involvement of the Resolution orthogneiss, and SW part of the Malaspina pluton (Fig. 3), in the domes (Fig. 9) indicates that they developed during and/or after the emplacement of both units.

Two distinguishing characteristics of the Breaksea domes are the steep, concentric orientations of the high-strain zones that surround them and patterns of L_2 mineral stretching lineations. The high-strain zones range in thickness from a few hundred meters to almost a kilometer wide (Fig. 9) and maintain their steep orientations where they wrap the sides of the domes. The plunges of L_2 mineral lineations range from near horizontal, mostly near dome tops, to greater than 80° in the steepest high-strain zones (Fig. 3B). Their trends swing a full 360°, forming a radial pattern within the concentric high-strain zones (Fig. 3B).

Kinematic indicators within L_2/S_2, including asymmetric shear bands in high-strain zones (Fig. 7E), show a spatially complex pattern of displacements parallel to L_2 mineral lineations. The steep orientations of the lineations in high-strain zones indicate near-vertical, dome-side-up displacements (cf. Betka and Klepeis, 2013) balanced by the downward movement of material in high-strain zones external to the domes. Near dome roofs, the L_2/S_2 fabric records the movement of material away from dome interiors, which also is compatible with subvertical displacements.

Doubtful Sound Shear Zone

The Doubtful Sound shear zone consists of thin (10–100 m) bands of hornblende-clinozoisite-biotite gneiss that form high-strain zones (D_3) up to 1 km thick (Figs. 4, 5A, and 5B). The thickest zones occur at the northern end of Crooked Arm, where high strains are indicated by the degree of transposition of older L_1/S_1 and L_2/S_2 fabrics, high densities of shear bands, the presence of tight-isoclinal folds, and an abundance of mylonite. Klepeis et al. (2007) showed that these areas record vertical flattening and horizontal stretching within conjugate-style arrays. These shear zones record the localization of deformation at the margins of the Malaspina intrusion, where competency contrasts with the Deep Cove gneiss must have been significant.

At the regional scale, the Doubtful Sound shear zone is folded into a series of gentle domes and basins with ~20 km wavelengths (Figs. 4 and 5). At Crooked Arm, it dips mostly N and NE, although locally it is folded into a series of second-order antiforms and synforms. To the west and east of this locality, it is folded into doubly plunging antiforms (Fig. 5A). Between Crooked Arm and Breaksea Sound, the shear zone arches into an E-W–trending antiformal dome (Fig. 5E) that is paired with a S-plunging synform (Fig. 5C). This synform tightens southward into Wet Jacket Arm (Fig. 5D). The southernmost branch of the shear zone is exposed on the south shore of Breaksea Sound (Fig. 4), where it breaks into narrow (≥10 m) strands that die out to the west.

Lineation patterns, which record a spread of trends to the NE and SW (Fig. 4A), reflect both the effects of the regional domes and basins and the deflection of material around lozenges of older gneiss. Despite the scatter, L_3 is readily distinguished from L_2 on the basis of both mineral assemblage and orientation. When compared at the same locality, L_3 consistently shows more northerly trends than L_2. This distinction suggests that, although D_2 and D_3 shear zones record similar directions of bulk flow at the regional scale, D_3 records local differences in both flow direction and dominant shear sense, as well as metamorphic grade and structural style.

Resolution Island Shear Zone

The Resolution Island shear zone is the largest of a series of upper-amphibolite-facies high-strain zones that occur at Breaksea entrance (Fig. 4). The shear zone consists of a 200–500-m-thick section of lineated (L > S) hornblende-clinozoisite-biotite gneiss that wraps around the eastern side of dome 2 on Resolution Island (Fig. 9) and cuts the Deep Cove gneiss. For this study, we mapped the continuation of the shear zone across Break-

sea Sound to the NE, where it deforms the western Malaspina pluton and breaks into bands that step eastward (Fig. 4).

Several characteristics distinguish the Resolution Island shear zone from the Doubtful Sound shear zone. First, upper-amphibolite-facies foliations (S_3) in the former show more geometric complexity, including curved, highly variable dips and near-vertical orientations. Second, although many hornblende and plagioclase lineations (L_3) plunge gently toward the SW and NE, groups that plunge to the NW, SSE, and S also are common (Fig. 4B). Betka and Klepeis (2013) showed that this variability in both foliation and lineation orientations results from the deflection of the L_3/S_3 fabric around the sides and tops of dome 2 (their Figs. 8 and 9). These deflections give the shear zone a curved structure that mimics the geometry of the Breaksea gneiss domes.

The kinematics of the Resolution Island shear zone also are distinctive and influenced by the curved structure of the domes. At dome roofs, where high-strain zones dip gently, top-down-to-the-SSW and -NNE displacements are most common. At the sides of domes, where high-strain zones dip steeply, strike-slip and oblique-slip displacements are common. On Resolution Island, for example, the Resolution Island shear zone dips moderately to the S and SE and records mostly sinistral strike-slip motion with a component of top-to-the-NNE displacement (i.e., oblique-normal motion; cf. Betka and Klepeis, 2013). This style contrasts with the down-dip, normal motion recorded in the Doubtful Sound shear zone.

U-Pb ZIRCON GEOCHRONOLOGY

Methods

We dated 10 zircon-bearing samples from Breaksea and Doubtful Sounds (Fig. 11) to evaluate the absolute ages of magmatism, metamorphism, and deformation (Fig. 12). Nine samples were analyzed at the U.S. Geological Survey (USGS)–Stanford University SHRIMP-RG facility, and one at the University of Arizona LaserChron Center. The data are tabulated in supplementary Tables S1–S4 (see footnote 1). Sample locations and interpreted dates are shown in Figures 2–4. Concordia diagrams and error-weighted average age plots are shown in Figure 11 and summarized in Figure 12. Descriptions of the methods, including cathodoluminescence images, chondrite-normalized REE abundances, and titanium-in-zircon temperatures, are presented in the supplementary data file (see footnote 1).

Samples and Results

Breaksea Sound

Two samples from Hāwea Island (Fig. 9A) give the timing of igneous crystallization and metamorphism in the Breaksea orthogneiss. Sample 1333E (Figs. 11A and 11B) is a metadioritic garnet granulite that was interlayered with garnet pyroxenite. Zircons are large (>200 µm) and euhedral with relatively high (>1.0) Th/U ratios, suggesting they are igneous (supplementary Fig. S3 [see footnote 1]). Twelve SHRIMP-RG spot analyses of 12 separate zircons yielded an error-weighted average $^{206}Pb/^{238}U$ age of 122.3 ± 1.9 Ma (mean square of weighted deviates [MSWD] = 3.7). Three spot analyses give younger dates of 113.2–119.13 Ma and have high common/radiogenic Pb values. These spot analyses may have overlapped a common-Pb–rich phase, or the zircons may have experienced Pb loss related to later magmatism and/or granulite-facies metamorphism. We therefore rejected them from our weighted average age determination. The remaining nine zircons yielded an age of 123.2 ± 1.3 Ma (MSWD = 1.7; Fig. 11B).

Sample 1333D (Figs. 11C–11D) is a hornblende amphibolite from a shear zone (D_3) that cuts the Breaksea orthogneiss. Cathodoluminescence imaging revealed the presence of dark-gray cores that are embayed and overgrown by bright, luminescent rims (supplementary Fig. S2 [see footnote 1]). Two SHRIMP-RG spot analyses yielded core dates similar within error to those in sample 1333E (122.7–117.2 Ma), and another has a younger date of 110.3 Ma. All cores have Th/U values >1.0. In contrast, 12 SHRIMP-RG spot analyses from rim domains yielded dates from ca. 103 Ma to ca. 57 Ma, and Th/U values <0.2. Titanium-in-zircon thermometry of the luminescent rim domains gives an average temperature of ~615 °C. The weighted average age of all 12 luminescent rim domains is 85.7 ± 6.8 Ma (MSWD = 1.9). Three spots that yielded the young dates of 57–69 Ma have large errors (>9 m.y., 1 standard deviation [SD]; three white error ellipses in Fig. 11C). Excluding these dates as outliers gives an error-weighted average age of 88.8 ± 4.7 Ma (MSWD = 0.77). Both dates are viable for the amphibolite-facies fabric. We prefer the latter date because it lowers the MSWD and weights higher-precision data spots.

Sample 13204 (Figs. 11E and 11F) is from a deformed garnet-bearing felsic dike that intruded a pod of metabasic gneiss in a high-strain area of the Resolution orthogneiss (Figs. 3 and 9A). The dike both cuts a penetrative granulite-facies S_2 foliation and also is folded within it (Fig. 7D), indicating that it intruded during D_2. Thin, retrograde upper-amphibolite-facies shear zones also cut the dike, indicating that it was emplaced prior to D_3. Zircon grains from the dike range in size from 100 to 225 µm and display both sector and oscillatory zoning patterns (supplementary Fig. S3 [see footnote 1]). Eleven spots on 11 zircons give a weighted average age of 113.8 ± 3.4 Ma (MSWD = 3.0). Two spots give dates of 117.9 and 120.7 Ma and probably represent inheritance. The remaining nine zircons give an average igneous crystallization age of 109.4 ± 2.5 Ma (MSWD = 0.84; Fig. 11F), indicating that partial melts crystallized within D_2 shear zones at this time.

Sample 13118A (Figs. 11G and 11H) is from an unfoliated pegmatite dike that is folded within the Doubtful Sound shear zone along Breaksea Sound (Fig. 4). The analysis of 12 zircon grains yielded two Proterozoic populations (Figs. 11G and 11H) with peaks at ca. 550 Ma and ca. 1080 Ma. No Cretaceous zircon was present. Since no Precambrian rocks are exposed in New Zealand, the Proterozoic zircon probably was derived from the Australian or East Antarctica cratons (Mortimer et al., 1999). The results suggest that Deep Cove gneiss underlies the Malaspina pluton in this region.

Sample 0649 (Figs. 11I and 11J) is from an undeformed, postkinematic pegmatite dike that cuts the Resolution Island shear zone at Breaksea entrance (Fig. 4). The sample was collected to place an upper limit on the age of D_3 at Breaksea entrance. The analysis of 21 zircon grains yielded a uniform population (Fig. 11I) and an average igneous crystallization age of 89.3 ± 1.8 Ma (MSWD = 0.36; Fig. 11J), indicating that shear zone deformation had ceased by this time.

Doubtful Sound

Sample 1241 is a hornblende diorite gneiss interlayered with screens of Deep Cove gneiss at Crooked Arm (Fig. 2). This sample was collected to determine the age of the intrusive sheets that make up the roof of the Malaspina pluton. Analysis of 12 zircons yielded a date of 116.2 ± 1.4 Ma (MSWD = 1.9). One spot analysis was slightly older (120.4 Ma) and was rejected as a likely xenocryst. The remaining 11 zircons yielded an age of 115.9 ± 1.2 Ma (MSWD = 1.5; Figs. 11K and 11L), which we consider to be the best age for igneous crystallization.

Samples 1256 (Figs. 11M and 11N) and 1254 (Figs. 11O and 11P) are from pegmatitic dikes within the Doubtful Sound shear zone (Fig. 4). The former is from a syntectonic dike that both cuts S_3 in the shear zone and is folded within it, indicating that it intruded during D_3. The latter is from an undeformed dike that cuts across the shear zone at high angles. Both dikes contain a range in zircon dates, where the youngest population is

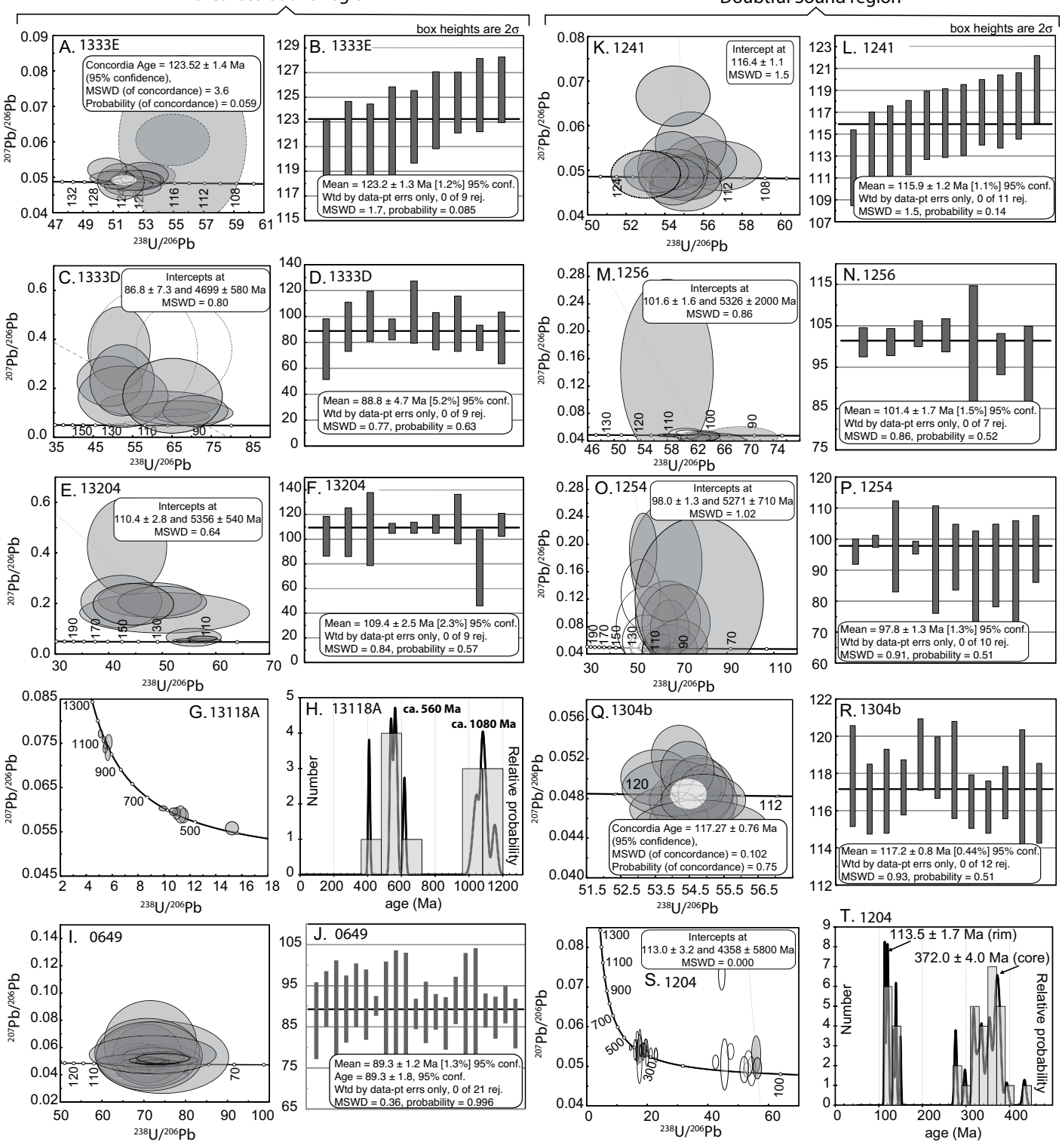

Figure 11. U-Pb zircon geochronology. Samples are from the Breaksea (A–J) and Doubtful Sound (K–T) regions (locations in Figs. 2, 3, and 4). Error ellipses in Tera-Wasserberg concordia plots (A, C, E, G, I, K, M, O, Q, S) and box heights in plots of calculated means (B, D, F, J, L, N, P, R) are 2σ. Plots in Figures 11H and 11T are age vs. probability diagrams. Dashed ellipses distinguish zircon cores in Figures 11A, 11C, 11K, and 11M. White ellipses in Figure 11C are excluded from the age calculations. White ellipses in Figures 11M and 11O are xenocrystic. MSWD—mean square of weighted deviates.

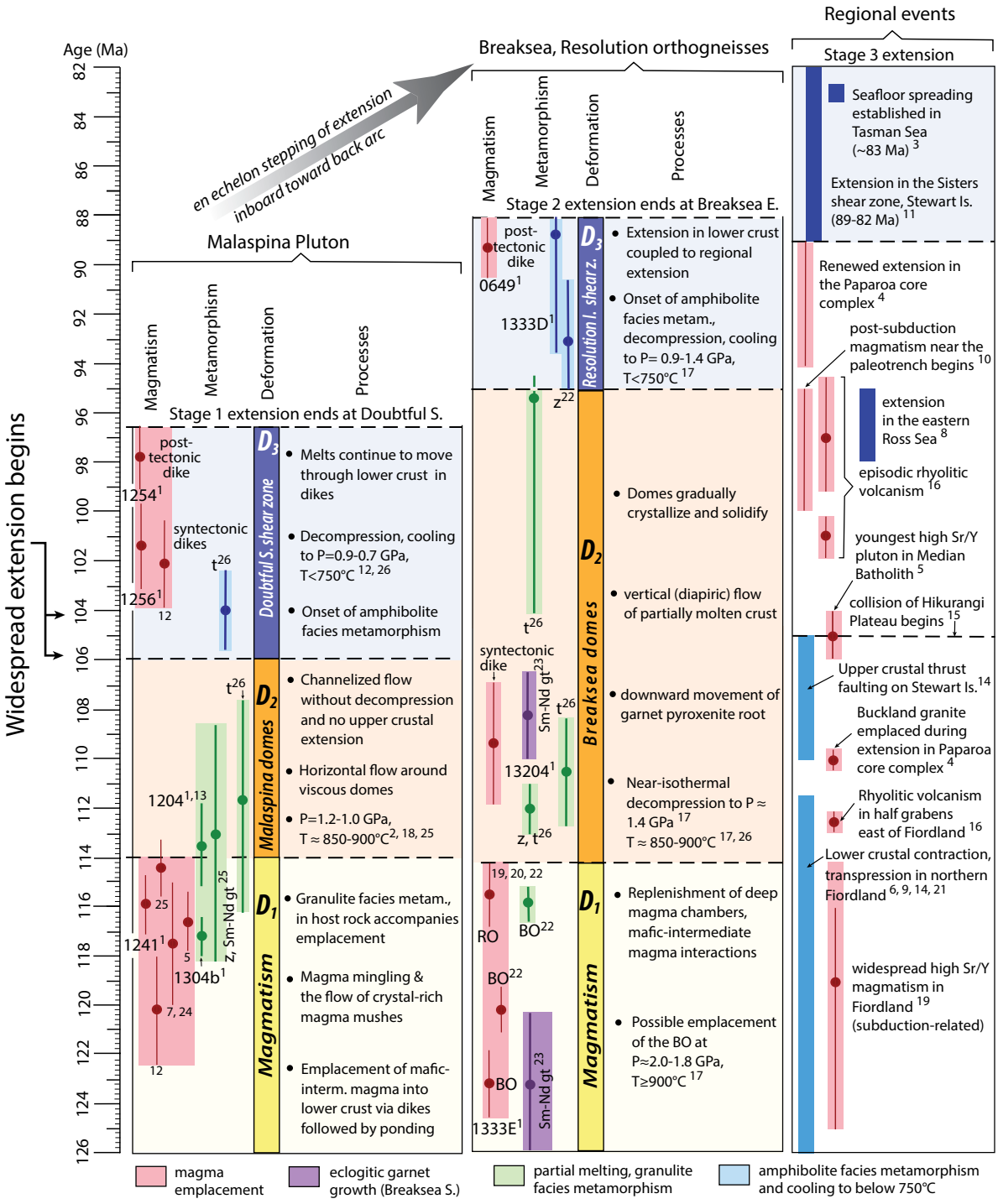

Figure 12. Time (vertical axis) vs. space (horizontal axis) diagram summarizing geochronologic data and tectonic events in central Fiordland and adjacent areas. The three columns show the Malaspina pluton on the left, the Breaksea and Resolution orthogneisses (BO and RO, respectively) in the middle, and regional events on the right. All ages are U-Pb zircon (z) determinations except where noted (t—titanite). Error bars are 2σ. Diagram shows that horizontal flow (D_2) in the Malaspina domes was short-lived, whereas vertical (diapiric) flow (D_2) in the Breaksea domes lasted longer. During D_3, extensional shear zones migrated toward the back arc where seafloor spreading began. Data sources: 1—this study; 2—Gibson and Ireland (1995); 3—Gaina et al. (1998); 4—Spell et al. (2000); 5—Tulloch and Kimbrough (2003); 6—Klepeis et al. (2004); 7—Hollis et al. (2004); 8—Siddoway et al. (2004); 9—Marcotte et al. (2005); 10—Mortimer et al. (2006); 11—Kula et al. (2007); 12—Klepeis et al. (2007); 13—King et al. (2008); 14—Allibone and Tulloch (2008); 15—Davy et al. (2008); 16—Tulloch et al. (2009); 17—De Paoli et al. (2009); 18—Allibone et al. (2009a); 19—Allibone et al. (2009c); 20—Turnbull et al. (2010); 21—Scott et al. (2011); 22—Hout et al. (2012); 23—Hout et al. (2013); 24—Sadorski et al. (2013); 25—Stowell et al. (2014); 26—Schwartz et al. (2016).

distinguished by both Th/U ratio and age (older populations indicated by white ellipses in Figs. 11M and 11O). In sample 1256, the youngest population (seven grains) yielded an average age of 101.4 ± 1.7 Ma (MSWD = 0.86; Fig. 11N). These results indicate that deformation in the Doubtful Sound shear zone had initiated by 101.4 ± 1.7 Ma. The youngest population in sample 1254 (seven grains) yielded an average age of 97.8 ± 1.3 Ma (MSWD = 0.9; Fig. 11P). These latter ages indicate that the deformation had terminated by 97.8 ± 1.3 Ma.

Sample 1304b (Figs. 11Q and 11R) is a garnet-bearing orthogneiss from the Deep Cove gneiss in the hanging wall of the Doubtful Sound shear zone (Fig. 3). The sample lies within the contact aureole of the Malaspina pluton. Cathodoluminescence imaging shows bright, oscillatory zoned cores that are commonly fractured and embayed (supplementary Fig. S2 [see footnote 1]). Overgrowths show weak oscillatory zoning. The analysis of 12 zircon rim domains yielded a concordant age of 117.2 ± 0.8 Ma (MSWD = 0.93; Fig. 11R). Chondrite-normalized REE abundance patterns show that the zircon grew in equilibrium with garnet (supplementary Fig. S2 [see footnote 1]). This date is identical to the crystallization age of the 118–115 Ma Malaspina pluton (Fig. 12; Sadorski, 2015), which links zircon and garnet growth to magma emplacement and contact metamorphism.

Sample 1204 (Figs. 11S and 11T) is a garnet-bearing orthogneiss from the Deep Cove gneiss at Hall Arm (Fig. 3). This sample also is from the contact aureole of the Malaspina pluton. Zircon is typically 100 µm in length and oblong in shape with poorly developed crystal facets. Cathodoluminescence imaging reveals a dominant population of bright and strongly zoned cores surrounded by thin (<10 µm), high-U oscillatory zoned rims (supplementary Fig. S4 [see footnote 1]). Rim domains commonly truncate oscillatory and sector zoning in core domains, suggesting secondary growth. Twenty core and rim spot analyses were conducted on zircons embedded in polished epoxy mounts. The thin rims proved difficult to isolate in polished epoxy mounts, and so 13 additional spot analyses were conducted by depth profiling (supplementary Fig. S5 [see footnote 1]) flat crystal faces embedded in indium. Results from both approaches yielded similar results, with dates ranging from ca. 434 to ca. 113 Ma. The dominant pre-Cretaceous peak (nine analyses) yielded a Devonian age of 372.0 ± 4.0 Ma (MSWD = 1.8; Fig. 11T). Two Cretaceous rims gave an age of 113.5 ± 1.7 Ma (MSWD = 0.03) and had Th/U values (~0.1) consistent with a metamorphic origin.

DISCUSSION

Structure of Lower Arc Crust

The three-dimensional structure of the study area provides a framework within which to discuss processes affecting the evolution of lower arc crust (Fig. 13). The main results include: (1) a 6-km-wide zone of steep (72°–90°) dikes within the NW part of the Malaspina pluton that penetrated, disrupted, and entrained older garnet pyroxenite of the Breaksea orthogneiss and fed zones of flat (<34°) dioritic intrusions up to 2 km thick (D_1); (2) the occurrence of narrow (0.2–1 km) thermal contact aureoles in all sectors of the study area that record high-grade metamorphism and crustal melting accompanying emplacement of the Malaspina pluton; (3) the simultaneous formation of two styles of migmatitic gneiss domes; (4) the occurrence of thick (1–2 km) granulite-facies shear zones that surrounded the domes, and recorded different combinations of vertical and horizontal flow (D_2); (5) sense-of-shear indicators and mineral stretching lineations that record radial flow in the Breaksea domes, and bidirectional flow in the Malaspina domes; and (6) the discovery that the Doubtful Sound shear zone and Resolution Island shear zone represent two temporally migrating extensional systems (D_3) that young toward the back arc.

The geometry of D_1 and D_2 features is summarized in Figures 10 and 13. The latter emphasizes the mushroom-shaped structure of the Malaspina pluton, which is characterized by steeply and moderately dipping zones that twist smoothly into gently dipping zones. The gently dipping portions lie below a roof of Paleozoic host gneiss that records multiple episodes of magma injection, crustal melting, and granulite-facies meta-

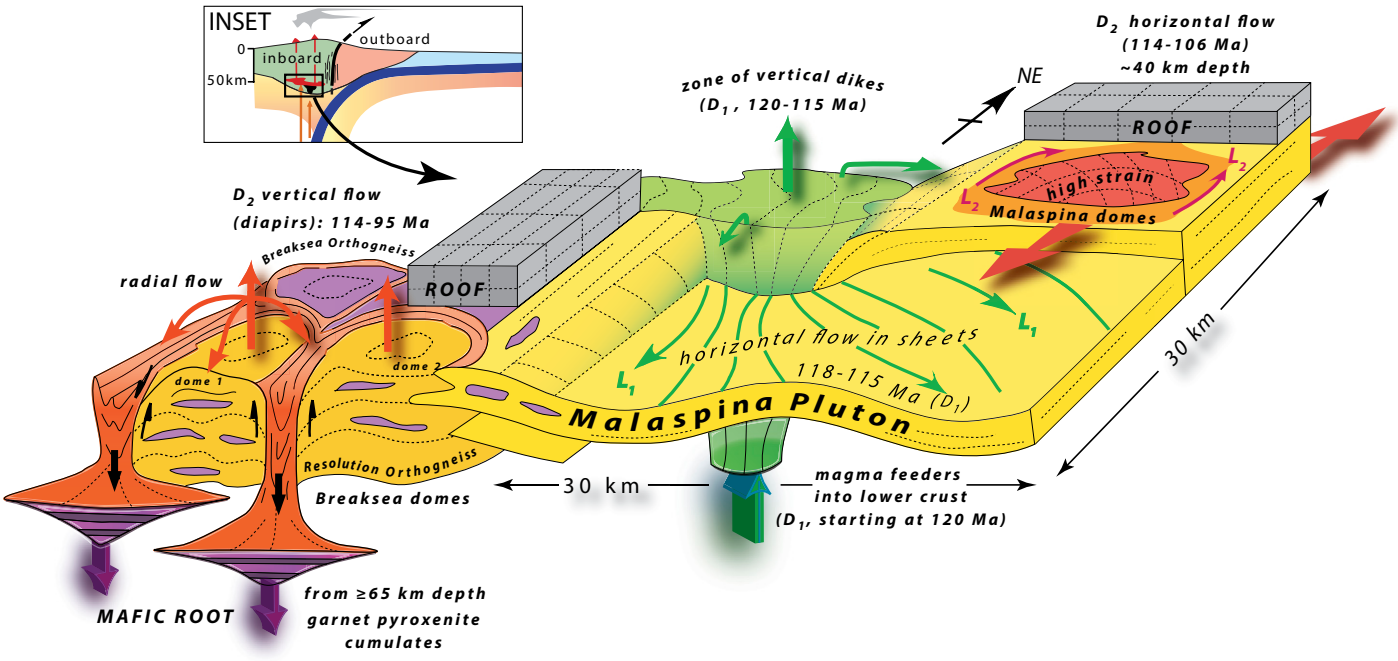

Figure 13. Three-dimensional block diagram of the lower crust showing spatial relationships among zones of vertical and horizontal flow during and after D_1 magmatism and prior to the development of D_3 shear zones.

morphism but little deformation during pluton emplacement. Figure 10B shows the three-dimensional structure of the Malaspina gneiss domes in detail. This area records two distinctive flow patterns at depths of ~40 km: (1) an early (D_1) period of mostly E-W– and SE-NW–trending viscous flow in crystal-rich magmas following their emplacement and, (2) later, mostly ENE-WSW subhorizontal flow in migmatitic high-strain zones (D_2). Both patterns contrast with the mostly vertical flow in the Breaksea domes. Figure 10B also shows the dome-shaped Doubtful Sound shear zone, which dies out to the south.

These results indicate that the transitions from mostly vertical to mostly subhorizontal planar fabrics interpreted below depths of ~25 km in other Cordilleran arcs (e.g., Kidder et al., 2003; Otamendi et al., 2012) need not be smooth ones in three dimensions. The Fiordland section agrees well with observations in the Northern Cascades (Miller et al., 2009) and shows that zones of steeply and gently dipping planar fabrics evolved simultaneously at different depths (40–65 km) and horizontally within different sectors of the lower crust (Fig. 13). This heterogeneity, and the different flow styles also support the interpretation that the deep parts of arc crust undergo a viscous overturning that promotes the vertical transport of material to shallow depths (Saleeby et al., 2003; Rey et al., 2009; Kruckenberg et al., 2011) while melts in other areas either crystallize at depth or are removed in batches by steep dikes. This example highlights the heterogeneous, domainal preservation of structures in lower-crustal MASH zones, which allowed us to track mass-transfer processes over a substantial (~35 m.y.) time period from ca. 123 to ca. 88 Ma.

Magmatism and Lower-Crustal Growth (D_1)

The geologic history of the Breaksea orthogneiss is significant because it appears to represent the deepest (~65 km) known field exposures of garnet-pyroxenite cumulates formed from an intermediate, mostly monzodioritic magma at the base of a continental arc. The Kohistan arc in Pakistan records comparable paleodepths (0–55 km; Jagoutz and Behn, 2013), but that section represents a transitional oceanic arc where mafic-ultramafic cumulates formed from mafic rather than intermediate magmas at lower pressures (1.0–1.2 GPa). Instead, the mafic and ultramafic components of the Breaksea orthogneiss may be most similar to small (≤15 cm), rare xenoliths of garnet clinopyroxenite reported in Miocene volcanic rocks in the Sierra Nevada Batholith (Ducea, 2002; Lee et al., 2006). These xenoliths record a pressure range of 1.2–2 GPa and have been interpreted to indicate that continental arc roots below 50 km are populated by plagioclase-free residual and/or cumulate material rich in clinopyroxene, amphibole, and/or garnet (Saleeby et al., 2003; Ducea et al., 2015b). The Fiordland exposures support the presence of garnet-pyroxenite cumulates and residues in thick arc roots, although they also indicate that intermediate magmas, including plagioclase-rich hornblende diorite, are abundant.

The zircon ages from sample 1333E show that the emplacement of the Breaksea orthogneiss occurred at 123.2 ± 1.3 Ma (Fig. 11B), although zircon ages reported by Hout et al. (2012) allow residual melts to have persisted until 120.2 ± 1.0 Ma. Emplacement of the Malaspina pluton appears to have begun as early as ca. 120 Ma in its NW sector (Klepeis et al., 2007), but mostly occurred at 118–115 Ma (Fig. 12; Sadorski et al., 2013; Sadorski, 2015). The 115.9 ± 1.2 Ma zircon age from a dioritic sheet near the roof of the unit (Fig. 11L) falls within this range and highlights the intrusion's multistage growth history. Stowell et al. (2014) also reported the occurrence of ca. 114 Ma dikes along with the older (ca. 120 Ma) ones in the NW area of the pluton. The spatial distribution of all ages is compatible with an emplacement model whereby steep dikes in the NW area penetrated and disrupted the Breaksea orthogneiss and fed sheets that ponded within the Deep Cove gneiss (Fig. 13). Similar ages (115.5 ± 1.3 Ma) from the Resolution orthogneiss (Hout et al., 2012) indicate that these two units represent a major replenishment of hornblende diorite into a deep crustal magma chamber previously occupied by the Breaksea orthogneiss.

Within a regional context, the intrusion of the Malaspina pluton and Resolution orthogneiss coincided with the emplacement of another lower-crustal body composed mostly of hornblende diorite: the Misty pluton (Fig. 2). Together, these three intrusions now occupy a surface area of >1260 km^2 (at least 2500 km^3 using a minimum thickness of 2 km from visible sills) and represent magma that also was emplaced mostly from 118 to 115 Ma (Sadorski et al., 2013; Sadorski, 2015). Their combined ages and regional extent allow up to 70% of the lower crust in central Fiordland to have been emplaced within a relatively short (3–4 m.y.) burst. Other high-flux igneous events in arcs have been identified mostly from the study of upper- and middle-crustal exposures (e.g., Petford et al., 1996; Saleeby et al., 2003; Paterson et al., 2011; Ducea et al., 2015a). Fiordland augments this work by providing a record of an igneous flare-up that resulted in significant lower-crustal growth as subduction either slowed or stopped.

In addition to crustal thickening and lower-crustal growth, the igneous burst had several other important consequences for the evolution of the Cretaceous arc. First, it led to the breakup and assimilation of older mafic units, including garnet pyroxenite. Second, it thermally and mechanically rejuvenated the base of the arc, which led to high-grade metamorphism, melting of the root, and the circulation of melts within the crust. The metamorphic ages from sample 1304b represent one of the oldest episodes (117.2 ± 0.8 Ma) of Mesozoic granulite-facies metamorphism yet found within or near the Malaspina pluton (Figs. 11R and 12). These ages, and identical crystallization ages from the pluton, link the metamorphism to magma emplacement. In the context of published dates (Fig. 12), these results indicate that the thermal effects of the flare-up were widespread, with high-grade metamorphism and partial melting lasting at least 5 m.y. (Stowell et al., 2014) after magma replenishment.

The mechanical consequences of rejuvenation are illustrated by the D_1 to D_2 transition, when deformation mobilized and concentrated felsic melts in high-strain zones, and formed the Malaspina and Breaksea gneiss domes (Figs. 3 and 12). This deformation, which we explore further later herein, provides a mechanism for the hybridization of melts derived from different parts of the lower crust and forms an important part of the deep crustal MASH zone. Some of these melts appear to have escaped the lower crust in dikes and veins (Figs. 7D and 8B–8E), which may help to explain the compositional diversity observed in upper-crustal plutons (Allibone et al., 2009c).

Last, the characteristics of this early phase of Fiordland's Cretaceous history support interpretations (e.g., Ducea et al., 2015b) that arcs of long duration generate hot, thick lower crust that is especially prone to remelting, reactivation, and the downward movement of dense mafic-ultramafic material. The breakup of older units, and the mobilization of crustal melts after new magma is introduced, appears to be a primary density sorting mechanism that helps to concentrate dense mafic-ultramafic cumulates and residues at the base of the crust and promotes the foundering of thick arc roots. This process lends support to the idea that most geochemical diversity in continental arcs is achieved within the lower crust (Hacker et al., 2015; Jagoutz and Kelemen, 2015).

Lateral and Vertical Flow of Partially Molten Lower Crust

Malaspina Gneiss Domes—Lateral (Channelized) Flow

Structural relationships. The Malaspina gneiss domes are defined in part by the curved trajectories of magmatic foliations (S_1; Fig. 2) that record variable degrees of crystal exchange between magma bodies of

mafic, ultramafic, and intermediate composition (Figs. 8A–8C). These foliations, and the domes, formed late in the crystallization history of the pluton, when it was viscous, crystal rich, and deforming near its solidus (D_1). This interpretation is in agreement with other studies that suggest magmatic foliations and lineations in crystallizing plutons are easily reset and typically record only the last stage of hypersolidus deformation (e.g., Paterson et al., 1998; Yoshinobu et al., 2009; Webber et al., 2015).

The continued evolution of the domes during D_2 is indicated by their relationship to high- and intermediate-strain zones. Migmatitic, granulite-facies shear zones envelop the domes (Figs. 3, 5, and 10) and record the flow of partially molten crust around them (Figs. 8E–8G). This partitioning of strain, and the preservation of the older (S_1/L_1) fabric in dome interiors, suggest that the effective viscosity of the domes was increasing as the shear zones formed. The fact that the long axes of three of the five domes parallel the L_2 stretching directions and are orthogonal to the older (L_1) lineations (Figs. 3A, 10B) suggests that their orientations reflect D_2 flow.

The spatial distribution and geometry of D_2 structures (Figs. 2, 3, 5, and 10), and the kinematics of flow, also help to constrain the dome-forming mechanisms. Structural relationships allowed us to eliminate an interpretation involving two interfering fold sets resulting from orthogonal directions of shortening. We did not, for example, observe evidence of NE-SW shortening parallel to L_2, nor the presence of steep, axial planar foliations expected for interfering folds (Forbes et al., 2004; Kim et al., 2007). Instead, the trajectories of mineral lineations (L_2) and foliations (S_2) indicate that the flow was mainly lateral (Fig. 3) within flat shear zones (Fig. 5). Linear ($L > S$ and $L = S$) fabrics and sense-of-shear indicators indicating both top-to-the-ENE and -WSW displacements suggest a bidirectional flow field within a ≥200 km^2 area (Figs. 3, 10, and 13).

Structural data from the Deep Cove gneiss, which mantles the domes, also are informative. Intrusive relationships and the ages of partial melting, high-grade metamorphism, and magma emplacement all indicate that these rocks were in contact with the Malaspina pluton when the domes formed, as indicated by youngest metamorphic zircon rims in sample 1204 (ca. 113 Ma). However, the host gneiss lacks any evidence of pervasive D_2 deformation. This relationship suggests that contrasts in effective viscosity between the intrusion and its host rock helped localize the deformation within the Malaspina pluton.

Together, these observations establish the Malaspina domes as having formed initially late in the crystallization history of the Malaspina pluton after emplacement (D_1) and later by the lateral flow (D_2) of migmatitic crust in thin (1–2 km), flat granulite-facies shear zones (Fig. 10B). The lack of D_2 deformation in the surrounding host gneiss indicates that the D_2 flow occurred solely within the pluton beneath a roof that resisted deformation. Although the base is not exposed, we infer that layers of Paleozoic Deep Cove gneiss lie below the flat, eastern part of the Malaspina pluton, because late dikes (sample 13118A; Fig. 11H) emplaced into it picked up a Paleozoic signal and yield no Cretaceous dates. These characteristics agree favorably with other field criteria used for recognizing exhumed channels (e.g., Whitney et al., 2004; Godin et al., 2006; Vanderhaeghe, 2009), including: (1) a crustal package of low-viscosity material bounded by higher-viscosity rock, (2) pervasive shearing in the channel that was synchronous with partial melting, (3) foliations and mineral stretching lineations indicating lateral displacements dominated over vertical ones, and (4) coeval movement and opposite senses of motion on shear zones bounding the channel. They also contrast with observations in the Northern Cascades arc, where Miller et al. (2009) documented increased coupling and decreased rheological contrasts between plutons and their hosts with depth.

Although the Doubtful Sound shear zone (Fig. 5) records NE-SW horizontal flow in gently dipping shear zones that appears similar to D_2 flow, this structure does not appear to have contributed significantly to the formation of the Malaspina domes. High-strain zones (D_3) cut through the domes at their northern and eastern ends and also cut obliquely across the older L_1/S_1 fabric in areas that lack D_2 high-strain zones, such as in the NW quadrant (Fig. 5A). Thus, the domes are interpreted to be magmatic-anatectic hybrids formed during the final stages of D_1 and mostly during D_2. These observations also suggest that the D_3 and D_2 shear zones do not represent the upper and lower parts of a single structure, respectively.

Pressure-temperature-time (P-T-t) paths. Published information on the pressures and temperatures of high-grade metamorphism and partial melting during D_2 (summarized in Fig. 6) support the interpretation that the Malaspina domes formed by the horizontal flow of partially molten crust in channels. Pressure-temperature estimates for the peak of granulite-facies metamorphism at Crooked Arm using thermobarometry and pseudosection modeling are in the range 1.2–1.45 GPa and 850–900 °C (Hollis et al., 2004; Allibone et al., 2009b; Stowell et al., 2014). These calculations, and evidence that partial melts were mobilized within D_2 shear zones (Figs. 7F–7H), indicate that the Malaspina pluton was still deforming above its solidus as the shear zones formed. Because the metamorphism was synchronous with D_2 deformation, these estimates also record the conditions at which the high- and intermediate-strain zones formed.

Stowell et al. (2014) calculated new *P-T-t* paths for these rocks and showed that D_2 partial melting and granulite-facies metamorphism occurred at either constant pressure or involved small amounts of localized loading. The possibility of some local loading may be compatible with initial dome formation late in D_1 as magma ponded within the lower crust. The lack of decompression supports the conclusion that the flow of melt-laden crust below a relatively rigid roof of host rock during D_2 was mostly horizontal. Thus, the *P-T-t* path for D_2 indicates that this event was not yet accompanied by significant extensional denudation in the upper crust above the domes.

Published *P-T* estimates for rocks in the footwall of the Doubtful Sound shear zone show that the transition from D_2 to D_3 involved cooling to 550–650 °C and decompression from ≥1.2 to 0.7–0.9 GPa (Klepeis et al., 2007). The inferred temperatures are compatible with $^{206}Pb/^{238}U$ titanite dates that show upper-amphibolite-facies metamorphism in the shear zone involved cooling below ~730 °C (Schwartz et al., 2016; Fig. 12). The decompression suggests that extension of the upper crust became widespread during D_3 (Klepeis et al., 2007; Kula et al., 2007; Tulloch et al., 2009).

Geochronology. The age of the transition from deformation in a viscous, crystallizing magma during D_1 to deformation in migmatitic granulite-facies shear zones during D_2 is marked by the age of the oldest S_2 foliation in the shear zones that surround the domes. Stowell et al. (2014) reported nine Sm-Nd garnet ages from the Malaspina pluton that indicate partial melting occurred throughout the interval 116–111 Ma. The oldest reported garnet age of 115.6 ± 2.6 is from a few kilometers north of the high-strain zone we mapped at site 38 in Crooked Arm (Fig. 4). This age is indistinguishable from a zircon crystallization age obtained from inside the high-strain zone (Stowell et al., 2014) and another (115.9 ± 1.2 Ma) we obtained outside it (sample 1241; Figs. 2 and 11L). Using a combination of ages, Stowell et al. (2014) concluded that the interval between pluton emplacement and partial melting was <5 m.y., and probably <3 m.y. Because partial melting, garnet granulite-facies metamorphism, and D_2 deformation were synchronous, the D_1 to D_2 transition was equally rapid and had occurred by 114–113 Ma (Fig. 12). This interpretation is compatible with the 117–113 Ma range of metamorphic ages we obtained from samples 1304b and 1204 in the thermal aureole of the Malaspina pluton (Figs. 3, 11R, 11T, and 12).

The transition from D_2 to D_3 is marked by the age of the oldest S_3 foliation in the Doubtful Sound shear zone. An upper limit is provided by the age of dikes that both cut S_3 and are folded within it, indicating they were

emplaced during D_3. Sample 1256 shows that the transition occurred prior to 101.4 ± 1.7 Ma (Fig. 11N). This result agrees well with the age (102.1 ± 1.8 Ma) of another syntectonic dike collected a few kilometers to the NW (Klepeis et al., 2007). The error limits on these ages allow D_3 to have initiated prior to 104 Ma.

Titanite and metamorphic zircon dates reported by Schwartz et al. (2016) record initially high-temperature (900–750 °C) metamorphism at 116.2–107.6 Ma within thermal aureoles of the Malaspina pluton during and after its emplacement. This history was followed by lower-crustal cooling through ~730 °C and upper-amphibolite-facies metamorphism in the Doubtful Sound shear zone at 106–102 Ma. Older titanite dates (113.41 ± 0.4 Ma, 112.1 ± 0.3 Ma; Flowers et al., 2005) are not linked to S_3 and may form part of an earlier history of localized heating and cooling. The 106–102 Ma ages obtained by Schwartz et al. (2016) agree well with the age of the Doubtful Sound shear zone determined using syntectonic dikes, which indicate that the D_2 to D_3 transition occurred prior to 102.1 ± 1.8 Ma. Zircon dates from a posttectonic dike (Fig. 11P) indicate that the shear zone was abandoned by 97.8 ± 1.3 Ma (Fig. 12). Together, the age of this posttectonic dike and the 106–102 titanite ages obtained by Schwartz et al. (2016) allow a maximum of ~8 m.y. and a minimum of ~4.8 m.y. for upper-amphibolite-facies metamorphism and deformation (D_3) in the Doubtful Sound shear zone.

These observations allow a maximum of 8 m.y. for the duration of D_2 (114–106 Ma) in the Malaspina pluton (Fig. 12). The history aligns well with our interpretation of channelized horizontal flow because (1) it shows that the mechanism forming the Malaspina domes did not involve significant vertical transport of hot lower crust, (2) the flow was not accompanied by significant upper-crustal extension, and (3) any exhumation occurred at a slow rate. This is compatible with models of channel flow in the deep, hot roots of orogens (Godin et al., 2006; Jamieson and Beaumont, 2011), which predict slow cooling from peak metamorphic conditions.

Breaksea Gneiss Domes—Vertical (Diapiric) Flow

Structural relationships. The Breaksea domes display nearly concentric trajectories of migmatitic, granulite-facies foliations (S_2) that formed after, and possibly also during, emplacement of the ca. 115 Ma Resolution orthogneiss. Our data combined with those of Betka and Klepeis (2013) show that the high-strain zones that surround the domes display approximately radial patterns of mineral stretching lineations (L_2; Fig. 3B). These lineations, combined with sense-of-shear indicators, record the downward movement of material away from dome interiors and are compatible with near-vertical, dome-side-up displacements (Fig. 13). Doubly plunging folds (Fig. 9) record the interfolding of material between the domes during the flow. In addition, subdomes are common and indicate that density variations were important as the domes formed. All of these features conform to the predictions of diapiric flow (Whitney et al., 2004; Little et al., 2011; Kruckenberg et al., 2011; Betka and Klepeis, 2013). In this interpretation, D_2 flow and dome formation were driven by density contrasts between hot, high-melt-fraction crust in dome cores, and cooler overlying rock of the Deep Cove gneiss, and dense garnet pyroxenite. The relationships suggest that the diapiric rise of the hot dome cores was balanced by a sinking of dense garnet-pyroxenite crust within the arc root (Fig. 13).

Metamorphic mineral assemblages and minor migmatite in the Deep Cove gneiss indicate that these rocks were in contact with the Malaspina pluton at the time the domes formed. Daczko et al. (2009) showed that they contain mineral assemblages that persisted metastably at pressures of 1.2 GPa during magma emplacement. They also lack a record of pervasive deformation during D_2, suggesting that density and viscosity contrasts were high enough so that D_2 deformation was partitioned into the hot, partially molten crust of the Breaksea and Resolution orthogneisses. On the basis of these observations we infer that the intrusion of the Resolution orthogneiss and Malaspina pluton provided a mechanism for heating and melting that enhanced density contrasts and triggered diapiric flow.

Pressure-temperature-time paths. The pressure and temperature histories of the Breaksea orthogneiss (summarized in Fig. 6) support an interpretation of vertical (diapiric) flow. De Paoli et al. (2009) used compositional zoning in clinopyroxene and garnet to infer average conditions of $P \approx 1.8$ GPa and $T \approx 850$ °C for both mafic and intermediate layers, with an earlier history that most likely exceeded $T \approx 900$ °C and $P \approx 2.0$ GPa. The *P-T* conditions for the oldest assemblages were derived from the cores of garnet paired with mineral inclusions in omphacite and appear to reflect decompression from subtly higher-grade conditions during the evolution of igneous protoliths (De Paoli et al., 2009) either late in D_1 or early in D_2. A subsequent part of the *P-T* history is recorded by symplectites of sodic diopside and albitic plagioclase that partially pseudomorphed omphacite. These younger mineral assemblages record near-isothermal decompression to garnet granulite-facies conditions at $P \approx 1.4$ GPa (De Paoli et al., 2009) during D_2. Near-isothermal decompression supports diapirism because experiments (e.g., Fayon et al., 2004) show that this type of flow is an efficient means of transferring material upward without losing much heat.

The interpretation of near-isothermal decompression during D_2 also is compatible with metamorphic ages obtained using zircon and titanite by Hout et al. (2012) and Schwartz et al. (2016), respectively. These authors showed that several pulses of granulite-facies metamorphism accompanied and followed the emplacement of the Resolution orthogneiss (Fig. 12). The interpretation aligns well with the observation that steep, migmatitic high strains continued to form after this unit intruded. The relationships also suggest that much of the partial melting and high-grade metamorphism in the Breaksea orthogneiss (e.g., Figs. 7B, 7C, and 7G) were triggered by emplacement of the Resolution orthogneiss and Malaspina pluton.

The recrystallization of garnet granulite-facies mineral assemblages to form hornblende, biotite, and clinozoisite gneiss during retrograde metamorphism is characteristic of all D_3 shear zones. De Paoli et al. (2009) showed that this event at Breaksea entrance involved further decompression accompanied by cooling and hydration at 0.9–1.4 GPa and 650–750 °C. These characteristics are predicted for styles of flow involving mostly lateral displacements accompanied by shallow extension (Whitney et al., 2004). Thus, the interpretation is compatible with a change in the style of flow from D_2 to D_3, which involved a shift from mostly vertical to mostly lateral displacements. It also suggests that the Breaksea domes initially formed deeper than the Malaspina domes and their *P-T-t* histories converged late in D_3. This inference is compatible with our conclusion that extension stepped to the SW during D_3 (Fig. 12) and that both the Doubtful Sound shear zone and Resolution Island shear zone were at similar depths (25–30 km, 0.9 GPa) when the latter formed.

Geochronology. Zircon crystallization ages indicate that the Resolution orthogneiss intruded at 115.1 ± 1.3 Ma (Hout et al., 2012). The involvement of this unit in the domes places a lower limit on the timing of the D_1 to D_2 transition (Fig. 12). Zircon crystallization ages from a syntectonic dike (Figs. 11E and 11F) that both cuts S_2 and is folded within it record the movement of partial melts in high-strain zones until at least 109.4 ± 2.5 Ma (Fig. 12). Metamorphic zircon and titanite dates (110.4 ± 2.2 Ma, 110.5 ± 2.2 Ma) record high-temperature (840–900 °C) metamorphism at this time (Schwartz et al., 2016), indicating that vertical flow in the Breaksea domes overlapped in time with horizontal flow in the Malaspina domes (Fig. 12).

The upper limit of D_2 at Breaksea entrance is indicated by the age of the oldest S_3 foliation in the hornblende-biotite-clinozoisite gneiss

within the Resolution Island shear zone system. The metamorphic zircon date obtained from sample 1333D (Figs. 11C and 11D) records upper-amphibolite-facies metamorphism at ~615 °C in D_3 shear zones at 88.8 ± 4.7 Ma. This age is compatible with metamorphic zircon dates (92.7 ± 2.1 Ma, 93.0 ± 1.6 Ma) from hornblende orthogneiss obtained by Hout et al. (2012) and titanite $^{206}Pb/^{238}U$ dates and Zr-in-titanite temperatures reported by Schwartz et al. (2016), who showed that high temperatures (816 °C) in the Resolution orthogneiss lasted through 95.2 ± 8.9 Ma (Fig. 12). These results indicate that the Breaksea domes not only were deeper, but also remained hot and partially molten for longer (~19 m.y.) than the Malaspina domes. The onset of upper-amphibolite-facies metamorphism in D_3 shear zones at ca. 95 Ma also indicates that the Resolution Island shear zone formed after deformation in the Doubtful Sound shear zone had ceased (Fig. 12). A postkinematic dike (Figs. 11I and 11J) indicates that D_3 deformation in the Resolution Island shear zone was over by 89.3 ± 1.8 Ma (Fig. 12). We therefore interpret the age of upper-amphibolite-facies deformation (D_3) at Breaksea entrance to be 95–89 Ma using the metamorphic zircon dates obtained by Hout et al. (2012) as a lower limit and the postkinematic dike as an upper limit.

Origin and Regional Significance of the Flow Styles

Magma Crystallization and Flow during Regional Contraction

The NE part of the Malaspina pluton (Fig. 2) preserves an excellent record of the rheological transitions that occurred during the last stages of D_1 magmatism. The oldest dikes show evidence of mingling with their dioritic hosts while in a magmatic state (Fig. 8A). Younger dikes record the comagmatic exchange of material with their hosts at a time when viscosity contrasts were low and the pluton was becoming increasingly crystal rich (Fig. 8B). The youngest dikes are mostly unfoliated and truncate S_1 folia at high angles (Fig. 8C). Straight margins on these latter examples suggest high strain rates and enough solid material (≥45–50 vol% crystal) for the hosts to fracture (Huber et al., 2011) prior to the formation of D_2 shear zones at ca. 114 Ma. This increase in the effective viscosity of the magma most likely was achieved through combinations of crystallization, a mechanical sorting of crystals at rheological boundaries, and the removal of interstitial melts in veins and dikes (Vigneresse et al., 1996; Yoshinobu et al., 2009; Huber et al., 2011). All of these processes would have strengthened the pluton prior to D_2, allowing it to fracture and form penetrative mineral foliations and lineations.

This textural evidence supports the view that the S_1/L_1 fabric formed late in the crystallization history of the pluton and raises the possibility that it tracked regional strains. We tested this possibility by comparing L_1 flow directions from the NE part of the pluton, where the evidence for a rapidly strengthening crystal-rich mush is preserved best, with other intra-arc structures that formed at a similar time (Fig. 14A). In northern Fiordland, steep transpressional shear zones up to 15 km wide record contraction at high angles to the arc at 119–111 Ma, following emplacement of the Western Fiordland orthogneiss (Klepeis et al., 2004; Marcotte et al., 2005). The Caswell fold-and-thrust belt, which deforms the top of the Misty pluton (Daczko et al., 2002), and the Gutter shear zone on Stewart Island (Allibone and Tulloch, 2008) record similar shortening directions in the middle crust during this same interval. We inferred the shortening directions using average orientations of mineral stretching lineations and poles to foliations reported from these structures. All are similar to the average L_1 flow direction (Fig. 14A). These similarities suggest that L_1 reflects regional strains and supports the interpretation that the Malaspina pluton was emplaced into a contractional tectonic regime.

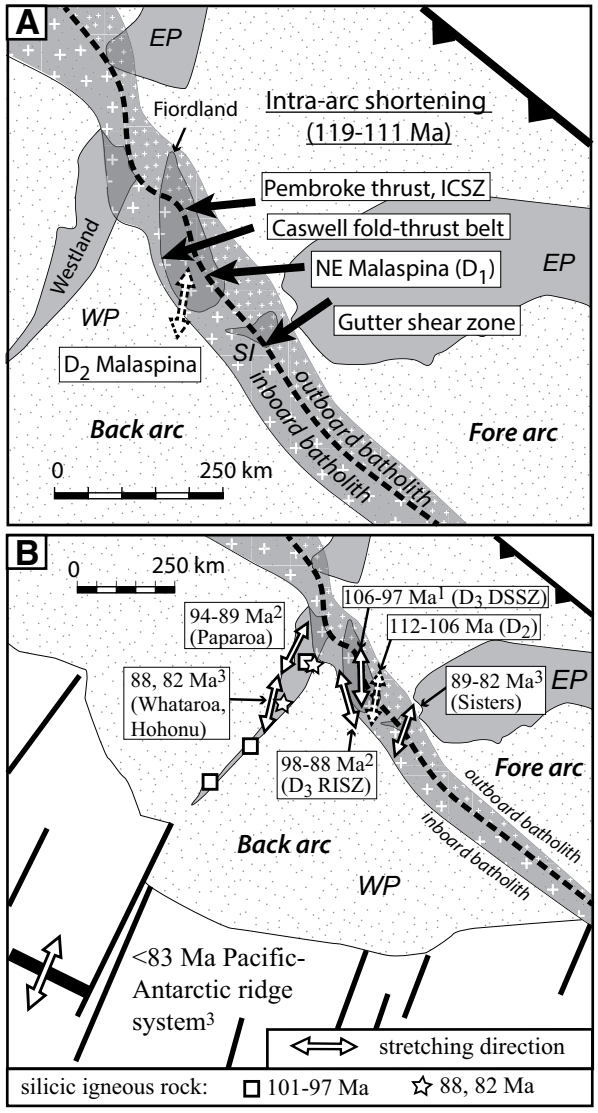

Figure 14. (A) Tectonic reconstruction showing average L_1 (140° in present-day coordinates) and L_2 (070°) stretching directions in the NE sector the Malaspina pluton and shortening directions in major contractional shear zones for the 119–111 Ma interval. Directions are plotted relative to the trend of the arc (020° in present-day coordinates). Fiordland location is after Tulloch et al. (2009). EP—Eastern Province, WP—Western Province, ICSZ—Indecision Creek shear zone. SI—Stewart Island. See text for discussion of data and sources. (B) Tectonic reconstruction for the 112–80 Ma interval showing a comparison of average stretching directions in D_2 (dashed arrow) and D_3 shear zones inside Fiordland with directions from extensional structures located adjacent to Fiordland (after Tulloch et al., 2009). DSSZ—Doubtful Sound shear zone, RISZ—Resolution Island shear zone. Superscripts refer to stages 1, 2, and 3 discussed in the text.

Initiation of Regional Extension

The onset of regional extension, leading to rifting and the breakup of Gondwana, generally is regarded to have occurred during the 105–100 Ma interval (Bradshaw, 1989; Mortimer, 2008). By ca. 111 Ma, transpression and thrusting in northern Fiordland had ceased (Klepeis et al., 2004; Marcotte et al., 2005; Scott et al., 2011), while some shal-

low thrust faulting continued south of Fiordland until ca. 105 Ma (Allibone and Tulloch, 2008; Fig. 12). High Sr/Y magmatism in the Median Batholith also ended at ca. 105 Ma (Tulloch and Kimbrough, 2003), shortly before postsubduction magmatism near the paleotrench began at 100–95 Ma (Mortimer et al., 2006). These relationships suggest that compression within the arc declined after ca. 111 Ma, and subduction had ended by ca. 100 Ma.

Our study indicates that the beginning of lower-crustal extension leading to rifting and continental breakup began at ca. 106 Ma with the formation of the Doubtful Sound shear zone. This structure represents the first unequivocal extensional shear zone that records decompression, cooling, and horizontal flow oblique to the trend of the arc (Fig. 14). These characteristics are compatible with the initiation of upper-crustal extension at this time, marking a major shift in the style of deformation within the arc (Fig. 12).

Gneiss Domes as Precursors to Rifting

Our analyses indicate that both the Malaspina and Breaksea domes began to form soon after a major burst of arc magmatism at 118–115 Ma and continued to evolve as intra-arc contraction declined after ca. 111 Ma. During this transition, the deformation circulated hot, partially molten material vertically and horizontally within the arc and aided lower-crustal cooling. The simultaneous development of contrasting flow styles further suggests that different rheologies and driving mechanisms governed the two sets of domes.

The geology of the Breaksea domes indicates that density sorting mechanisms and buoyancy forces were important at the base (~65 km) of the arc from at least ca. 114 Ma until ca. 95 Ma. This ca. 95 Ma date marks the change from vertical to lateral flow at cooler, upper-amphibolite-facies conditions during D_3 and is not associated with density sorting processes. Betka and Klepeis (2013) argued that the presence of garnet pyroxenite combined with crustal anatexis and high (850–900 °C) temperatures during D_2 enhanced density contrasts and lowered effective viscosities of dome interiors relative to cooler surrounding material. A thick, hot, weak lower crust thus appears to have allowed buoyancy forces to dominate and drive diapiric flow, which was balanced by sinking material (Fig. 13). In this context, the foundering of a dense root provided a mechanism of lower-crustal thinning at a time when contraction was diminishing and upper-crustal normal faulting was in its infancy.

At shallower depths (~40 km), the localization of subhorizontal shear zones (D_2) at the roof of the Malaspina pluton at 114–106 Ma also marks a change in the style of flow within the arc. Unlike the older L_1 flow directions from the same region, L_2 mineral lineations in D_2 shear zones record flow oblique to the arc (Fig. 14A) and are similar to the L_3 stretching directions in the younger D_3 extensional shear zones (Fig. 14B). This pattern suggests that the onset of lateral flow during D_2 (Figs. 13 and 14A) was a precursor to regional extension. The change in flow direction, along with the beginning of lower-crustal thinning by root detachment, indicates that the Breaksea and Malaspina domes both record a major shift in the dynamic evolution of the arc at ca. 114 Ma prior to the development of extension in the upper crust at ca. 106 Ma.

Evolution of Extension Leading to Continental Rifting

We recognize three distinctive stages of regional extension leading to continental breakup. Stage 1 extension (106–97 Ma) includes the Doubtful Sound shear zone, which was accompanied by decompression and cooling to below 730 °C (Fig. 14B). Localized pulses of amphibolite-facies metamorphism in the Doubtful Sound region at 106–102 Ma (Schwartz et al., 2016) marked the development of organized networks of these shear zones. These events also overlapped in time with an early phase of mid-crustal extension in the Paparoa metamorphic core complex (Fig. 12; Tulloch and Kimbrough (1989); Spell et al., 2000; Schulte et al., 2014).

Stage 2 extension (97–89 Ma) includes the Resolution Island shear zone, which records a migration of deformation toward the interior of Gondwana (Figs. 12 and 14B). This stage coincides with extensional shearing in the Ross Sea at 98–95 Ma (Siddoway et al., 2004) and the eruption of postsubduction magmas near the paleotrench (Mortimer et al., 2006). The timing of the former event is given by $^{40}Ar/^{39}Ar$ K-feldspar cooling ages, which show rapid cooling and mylonitization shortly after granitic magmatism in Marie Byrd Land. The lower plate of the Paparoa core complex (Fig. 14B) also records rapid cooling of its lower plate at 94–89 Ma ($^{40}Ar/^{39}Ar$ K-feldspar cooling ages), suggesting its footwall was breached by normal faulting at this time during either continued or renewed extension (Spell et al., 2000; Fig. 12). All of these features correspond to stage 1 rifting of Kula et al. (2007), which these authors linked to the northward propagation of the Tasman ridge (Fig. 1) between Zealandia–West Antarctica and East Antarctica–Australia.

Stage 3 extension (89–79 Ma) coincides with a period of rapid cooling ($^{40}Ar/^{39}Ar$ K-feldspar) in the Sisters shear zone (89–82 Ma) on Stewart Island (stage 2 of Kula et al., 2007) and emplacement of the Hohonu lamprophyre dikes (Tulloch et al., 2009; Fig. 14B). The end of the stage coincides with formation of the Pacific-Antarctic spreading ridge between Zealandia and West Antarctica (Figs. 1 and 14B), which records the formation of new ocean crust along the southeast margin of the Campbell Plateau at 83–79 Ma (Larter et al., 2002).

Collectively, these features attest to the broad distribution of extension leading to rifting and continental breakup after ca. 100 Ma. These stages illustrate that extension within Fiordland and other parts of Zealandia after 106 Ma gradually organized into shear zones and faults that, at least locally, migrated inboard over time (Fig. 14B). This migration does not appear to have been smooth, but, ultimately, the processes culminated in the formation of new ocean crust between Zealandia and the rest of Gondwana (Fig. 1). Tulloch et al. (2009) postulated that rifting gradually focused inboard of the Median Batholith because thin, cooler lithosphere there was more amenable to rupture than the hot thick crust inside the batholith. Several authors (Mortimer et al., 2006; Kula et al., 2007; Tulloch et al., 2009) also have postulated that the oblique orientation (20°–30°) of L_3 stretching directions relative to the paleotrench (Fig. 14B), and their parallelism to spreading centers, links them to the opening and propagation of these ridges.

Our data, which show the abandonment of the Doubtful Sound shear zone by ca. 97 Ma and formation of the Resolution Island shear zone at ca. 95 Ma (Fig. 14), further suggest that the spatial and temporal evolution of extension was strongly influenced by the rheological structure of the lower crust. Both the Breaksea and Malaspina domes record similar transitions from high-temperature deformation in migmatitic, granulite-facies shear zones (D_2) to cooler deformation and metamorphism at upper amphibolite facies (D_3). However, these transitions from D_2 to D_3 occurred at different rates in the two regions (Fig. 12). At the roof of the Malaspina pluton, the crust had cooled to below 730 °C, and strain had localized into the Doubtful Sound shear zone (D_3) by ca. 106 Ma. However, a similar transition occurred only after ca. 95 Ma in the Breaksea region (Fig. 12).

We suggest that the flat orientation of the roof of the Malaspina pluton and efficient thermal dissipation due to its broad surface area allowed D_3 deformation to localize there first as contraction waned and extension began at ca. 106 Ma. In contrast, the greater depth, smaller surface area, and relatively inefficient cooling and melt-extraction mechanisms allowed temperatures and melt volumes to remain high for longer in the Breaksea domes. By 97–95 Ma, strain hardening and cooling driven by extension would have increased the rigidity of the crust at the roof the Malaspina

pluton, leading to the abandonment of the Doubtful Sound shear zone and allowing extension to localize into the hotter, weaker crust of the Breaksea area. Thus, it appears that lower-crustal thinning by root detachment beginning at a. 114 Ma and cooling driven by extension beginning at ca. 106 Ma effectively ended buoyancy-driven diapirism at the base of the arc by ca. 95 Ma.

This interpretation is compatible with the results of thermomechanical simulations of sequentially activated normal faults at asymmetric rifted margins. Brune et al. (2014) concluded that rift migration is controlled by the thermal structure and variations in the viscosity of the lower crust. The time necessary for extension to localize into one dominant fault or shear zone is a function of the lower-crustal rheology, with weaker rheologies showing a more prolonged phase of initial distributed deformation. This relationship, whereby deformation follows the evolution of weak zones in the lower crust, explains the migration of D_3 shear zones in Fiordland. It also implies that zones of weakness caused by the vertical flow of hot material extended well into the middle crust (25–30 km), where they influenced the location of the Resolution Island shear zone.

The formation of lateral strength gradients in the lower crust as a result of variations in temperature, melt, and effective viscosity following an igneous flare-up also explains the diffuse, discontinuous style of extension in SW New Zealand. In contrast to systems where small numbers of faults each accommodate a large (≥30 km) amount of slip (e.g., Axen, 2004), Fiordland records a style whereby displacements in the lower crust were distributed across many thin shear zones. This style, and the abandonment of D_3 shear zones as deformation migrated toward the interior, explains why the extension did not significantly excise the lower crust or exhume it to upper-crustal depths (e.g., Klepeis et al., 2007; Allibone et al., 2009c). The relationships provide an example of how the presence of lateral variations in lower-crustal strength influenced the evolution of extension leading to continental breakup.

CONCLUSIONS

Structural analyses and U-Pb zircon geochronology show how mafic-intermediate magmatism and the flow of hot (850–900 °C), partially molten crust formed two contrasting styles of gneiss domes at different depths within a continental arc. Both sets of domes evolved simultaneously as arc magmatism, contraction, and subduction beneath Gondwana declined and were superseded by rifting and continental breakup. The Malaspina domes record lateral flow in 1–2-km-thick channels at ~40 km depth. Migmatitic high-strain zones envelop these domes and record bidirectional flow oblique to the trend (020°) of the arc. In contrast, the Breaksea domes record mostly vertical (dome-side-up) displacements with radial flow at the base of the arc (~65 km). This upward motion was balanced by the sinking of a dense root composed partly of garnet pyroxenite.

Both the Malaspina and Breaksea domes are magmatic and anatectic hybrids that began forming by viscous flow (D_1) in crystal-rich magmas after emplacement of the Malaspina pluton and Resolution orthogneiss. These plutons intruded the lower crust during a magma flare-up at 118–115 Ma that thermally and mechanically rejuvenated the base of the arc. Episodes of granulite-facies metamorphism and partial melting lasted up to 5 m.y. after magma emplacement. Melts derived from deep parts of the lower crust also were mobilized in the high-strain zones (D_2) that enveloped the domes after magma emplacement, providing a mechanism for melt hybridization in lower-crustal MASH zones.

After ca. 114 Ma, both sets of domes record a change from deformation close to the solidus, where granulite-facies metamorphism and crystal-plastic processes occurred in hot migmatitic shear zones (D_2), to cooler (<730 °C) deformation and metamorphism in narrow upper-amphibolite-facies shear zones (D_3). In the Malaspina domes, melt-enhanced deformation and channelized (lateral) flow (D_2) lasted 6–8 m.y. (114–106 Ma). In contrast, the Breaksea domes experienced a slower rate of cooling and solidification at the base of the arc, which remained hot and partially molten for up to 19 m.y. (114–95 Ma). The longer duration of hot, partially molten crust in the latter area enhanced density contrasts and buoyancy-driven flow, which promoted root foundering and diapirism. Root detachment helped thin the lower crust before regional extension became widespread after ca. 106 Ma.

Our preferred model of extension begins with the formation of the Doubtful Sound shear zone (106–97 Ma) at the roof of the Malaspina pluton (stage 1). This shear zone (D_3) records lower-crustal thinning, decompression with cooling, and horizontal flow oblique to the arc. The stage also coincided with an early phase of extension in the midcrustal Paparoa metamorphic core complex. Stage 2 (97–89 Ma) is represented by formation of the Resolution Island shear zone (D_3), which records the migration of extension toward the interior of Gondwana. This migration was driven by differences in the thermal structure and viscosity of the lower crust that resulted from magmatism and gneiss doming. The stage also coincides with the beginning of rifting in the eastern Ross Sea and the northward propagation of the Tasman spreading ridge. Stage 3 (89–79 Ma) includes a period of rapid cooling in the Sisters shear zone south of Fiordland, dike emplacement, and the formation of ocean crust at 83–79 Ma during opening of the Pacific-Antarctic spreading ridge. This model illustrates how the evolution of extension was influenced by both the rheological structure of the lower crust following an igneous flare-up and asymmetric rifting on propagating spreading ridges. In addition, the migration of shear zones toward the interior of Gondwana explains the diffuse, discontinuous style of extension within the batholith. This style involved displacements that were distributed across many high-strain zones rather than forming a small number of large-magnitude detachments capable of exhuming the lower crust to upper-crustal depths.

ACKNOWLEDGMENTS

Funding to support this work was provided by National Science Foundation (NSF) grants EAR-1119248 (Klepeis), EAR-1119039 (Stowell, Schwartz), and NSF EAR-1338583 (supporting the LaserChron laboratory at the University of Arizona). We thank Rose Turnbull, Richard Jongens, and Nick Mortimer at GNS (Dunedin) for discussions and assistance. Jeff Webber, Mike Ingram, Alice Newman, and Kathryn Dianiska conducted field work and contributed discussions and analyses. Doug MacLeod provided undergraduate research assistance, and Elena Miranda provided constructive comments. We thank the Department of Land Conservation for permission to sample. We also thank Robert Miller and an anonymous reviewer for constructive comments that improved this paper.

REFERENCES CITED

Allibone, A.H., and Tulloch, A.J., 2008, Early Cretaceous dextral transpressional deformation within the Median Batholith, Stewart Island, New Zealand: New Zealand Journal of Geology and Geophysics, v. 51, p. 115–134, doi:10.1080/00288300809509854.

Allibone, A.H., Jongens, R., Scott, J.M., Tulloch, A.J., Turnbull, I.M., Cooper, A.F., Powell, N.G., Ladley, E.B., King, R.P., and Rattenbury, M.S., 2009a, Plutonic rocks of the Median Batholith in eastern and central Fiordland, New Zealand: Field relations, geochemistry, correlation, and nomenclature: New Zealand Journal of Geology and Geophysics, v. 52, p. 101–148, doi:10.1080/00288300909509882.

Allibone, A.H., Milan, L.A., Daczko, N.R., and Turnbull, I.M., 2009b, Granulite facies thermal aureoles and metastable amphibolite facies assemblages adjacent to the Western Fiordland orthogneiss in southwest Fiordland, New Zealand: Journal of Metamorphic Geology, v. 27, p. 349–369, doi:10.1111/j.1525-1314.2009.00822.x.

Allibone, A.H., Jongens, R., Turnbull, I.M., Milan, L.A., Daczko, N.R., De Paoli, M.C., and Tulloch, A.J., 2009c, Plutonic rocks of western Fiordland, New Zealand: Field relations, geochemistry, correlation, and nomenclature: New Zealand Journal of Geology and Geophysics, v. 52, p. 379–415, doi:10.1080/00288306.2009.9518465.

Axen, G.J., 2004, Mechanics of low-angle normal faults, *in* Karner, G.D., Taylor, B., Driscoll, N.W., and Kohlstedt, D.L., eds., Rheology and Deformation of the Lithosphere at Continental Margins: New York, Columbia University Press, p. 46–91.

Betka, P.M., and Klepeis, K.A., 2013, Three-stage evolution of lower crustal gneiss domes at Breaksea entrance, Fiordland, New Zealand: Tectonics, v. 32, p. 1084–1106, doi:10.1002/tect.20068.

Blake, S., and Fink, J., 2000, On the deformation and freezing of enclaves during magma mixing: Journal of Volcanology and Geothermal Research, v. 95, no. 1–4, p. 1–8, doi:10.1016/S0377-0273(99)00129-8.

Bradshaw, J.D., 1989, Cretaceous geotectonic patterns in the New Zealand region: Tectonics, v. 8, p. 803–820, doi:10.1029/TC008i004p00803.

Bradshaw, J.Y., 1990, Geology of crystalline rocks of northern Fiordland; details of the granulite facies Western Fiordland orthogneiss and associated rock units: New Zealand Journal of Geology and Geophysics, v. 33, p. 465–484, doi:10.1080/00288306.1990.10425702.

Brune, S., Heine, C., Pérez-Gussinyé, M., and Sobolev, S.V., 2014, Rift migration explains continental margin asymmetry and crustal hyper-extension: Nature Communications, v. 5, p. 4014, doi:10.1038/ncomms5014.

Cao, W., Paterson, S., Memeti, V., Mundil, R., Anderson, J.L., and Schmidt, K., 2015, Tracking paleodeformation fields in the Mesozoic central Sierra Nevada arc: Implications for intra-arc cyclic deformation and arc tempos: Lithosphere, v. 7, no. 3, p. 296–320, doi:10.1130/L389.1.

Chavez, T., Grace, R., and Stowell, H.H., 2007, New garnet Sm-Nd evidence for Paleozoic metamorphism, Wet Jacket Arm Fiordland, New Zealand, Geological Society of America Abstracts with Programs, v. 39, no. 4, paper number 31–6.

Chin, E.J., Lee, C.T., Tollstrup, D.L., Xie, L.W., Wimpenny, J.B., and Yin, Q.Z., 2013, On the origin of hot metasedimentary quartzites in the lower crust: Earth and Planetary Science Letters, v. 361, p. 120–133, doi:10.1016/j.epsl.2012.11.031.

Clarke, G.L., Daczko, N.R., Klepeis, K.A., and Rushmer, T., 2005, Roles for fluid and/or melt advection in forming high-*P* mafic migmatites, Fiordland, New Zealand: Journal of Metamorphic Geology, v. 23, p. 557–567, doi:10.1111/j.1525-1314.2005.00594.x.

Clarke, G.L., Daczko, N.R., and Miescher, D., 2013, Identifying relic igneous garnet and clinopyroxene in eclogite and granulite, Breaksea orthogneiss, New Zealand: Journal of Petrology, v. 54, p. 1921–1938, doi:10.1093/petrology/egt036.

Daczko, N., Clarke, G.L., and Klepeis, K.A., 2001, The transformation of two-pyroxene-amphibole granulite to garnet granulite; simultaneous melting and fracturing of the lower crust, Fiordland, New Zealand: Journal of Metamorphic Geology, v. 19, p. 547–560, doi: 10.1046/j.0263-4929.2001.00328.x.

Daczko, N., Klepeis, K.A., and Clarke, G.L., 2002, Thermomechanical evolution of the crust during convergence and deep crustal pluton emplacement in the Western Province of Fiordland, New Zealand: Tectonics, v. 21, no. 4, p. 1–18, doi:10.1029/2001TC001282.

Daczko, N.R., Milan, L.A., and Halpin, J.A., 2009, Metastable persistence of pelitic metamorphic assemblages at the root of a Cretaceous magmatic arc—Fiordland, New Zealand: Journal of Metamorphic Geology, v. 27, p. 233–247, doi:10.1111/j.1525-1314.2009.00815.x.

Davy, B., Hoernle, K., and Werner, R., 2008, Hikurangi Plateau: Crustal structure, rifted formation, and Gondwana subduction history: Geochemistry Geophysics Geosystems, v. 9, Q07004, doi:10.1029/2007GC001855.

DeCelles, P.G., Ducea, M.N., Kapp, P., and Zandt, G., 2009, Cyclicity in Cordilleran orogenic systems: Nature Geoscience, v. 2, p. 251–257, doi:10.1038/ngeo469.

De Paoli, M.C., Clarke, C.L., Klepeis, K.A., Allibone, A.H., and Turnbull, I.M., 2009, The eclogite-granulite transition; mafic and intermediate assemblages at Breaksea Sound, New Zealand: Journal of Petrology, v. 50, no. 12, p. 2307–2343, doi:10.1093/petrology/egp078.

Ducea M.N., 2002, Constraints on the bulk composition and root foundering rates of continental arcs: A California arc perspective: Journal of Geophysical Research, v. 107, no. B11, p. 2304, doi:10.1029/2001JB000643.

Ducea, M.N., Paterson, S.R., and DeCelles, P.G., 2015a, High-volume magmatic events in subduction systems: Elements (Quebec), v. 11, p. 99–104, doi:10.2113/gselements.11.2.99.

Ducea, M.N., Saleeby, J.B., and Bergantz, G., 2015b, The architecture, chemistry, and evolution of continental magmatic arcs: Annual Reviews of Earth and Planetary Science, v. 43, p. 10.1–10.33, doi:10.1146/annurev-earth-060614-105049.

Fayon, A. K., Whitney, D.L., Teyssier, C., 2004, Exhumation of orogenic crust: Diapiric ascent versus low-angle normal faulting, *in* Whitney, D.L., Teyssier, C., and Siddoway, C.S., eds., Gneiss Domes in Orogeny: Geological Society of America Special Paper 380, p. 129–139, doi:10.1130/0-8137-2380-9.129.

Flowers, R.M., Bowring, S.A., Tulloch, A.J., and Klepeis, K.A., 2005, Tempo of burial and exhumation within the deep roots of a magmatic arc, Fiordland, New Zealand: Geology, v. 33, p. 17–20, doi:10.1130/G21010.1.

Forbes, C.J., Betts, P.G., and Lister, G.S., 2004, Synchronous development of type 2 and type 3 fold interference patterns: Evidence for recumbent sheath folds in the Allendale area, Broken Hill, NSW, Australia: Journal of Structural Geology, v. 26, p. 113–126, doi:10.1016/S0191-8141(03)00074-9.

Gaina, C., Muller, D.R., Royer, J.Y., Stock, J., Hardebeck, J., and Symonds, P., 1998, The tectonic history of the Tasman Sea: A puzzle with 13 pieces: Journal of Geophysical Research, v. 103, p. 12,413–12,433, doi:10.1029/98JB00386.

Getsinger, A., Rushmer, T., Jackson, M.J., and Baker, D., 2009, Generating high Mg numbers and chemical diversity in TTG magmas during melt segregation: Journal of Petrology, v. 50, p. 1935–1954, doi:10.1093/petrology/egp060.

Gibson, G.M., and Ireland T.R., 1995, Granulite formation during continental extension in Fiordland, New Zealand: Nature, v. 375, p. 479-482, doi:10.1038/375479a0.

Gibson, G.M., McDougall, I., and Ireland, T.R., 1988, Age constraints on metamorphism and the development of a metamorphic core complex in Fiordland, southern New Zealand: Geology, v. 16, p. 405–408, doi:10.1130/0091-7613(1988)016<0405:ACOMAT>2.3.CO;2.

Godin, L., Grujic, D., Law, R.D., and Searle, M.P., 2006, Channel flow, ductile extrusion, and exhumation in continental collision zones: An introduction, *in* Law, R.D., Godin, L., and Searle, M.P., eds., Channel Flow, Ductile Extrusion, and Exhumation in Continental Collision Zones: Geological Society of London Special Publication 268, p. 1–23, doi:10.1144/GSL.SP.2006.268.01.01.

Hacker, B.R., Kelemen P.B., and Behn, M,D., 2015, Continental lower crust: Annual Reviews of Earth and Planetary Science, v. 43, p. 6.1–6.39, doi:10.1146/annurev-earth-050212-124117.

Hildreth, W., and Moorbath, S., 1988, Crustal contributions to arc magmatism in the Andes of central Chile: Contributions to Mineralogy and Petrology, v. 98, p. 455–489, doi:10.1007/BF00372365.

Hollis, J.A., Clarke, G.L., Klepeis, K.A., Daczko, N.R., and Ireland, T.R., 2004, The regional significance of Cretaceous magmatism and metamorphism in Fiordland, New Zealand, from U-Pb zircon geochronology: Journal of Metamorphic Geology, v. 22, p. 607–627, doi:10.1111/j.1525-1314.2004.00537.x.

Hout, C., Stowell, H., Schwartz, J., and Klepeis, K., 2012, New $^{206}Pb/^{238}U$ zircon ages record magmatism and metamorphism in the crustal root of a magmatic arc, Fiordland, New Zealand: Geological Society of America Abstracts with Programs, v. 44, no. 7, p. 586.

Hout, C., Stowell, H., Schwartz, J.J., Klepeis, K., and Koenig, A.E., 2013, New garnet Sm-Nd ages record timing of eclogitic garnet growth in Fiordland, New Zealand: Geological Society of America Abstracts with Programs, v. 45, no. 7, p. 799.

Huang, Y., Chunakov, V., Mantovani, F., Rudnick, R.L., and McDonough, W.F., 2013, A reference Earth model for the heat-producing elements and associated geoneutrino flux: Geochemistry Geophysics Geosystems, v. 14, p. 2003–2029, doi:10.1002/ggge.20129.

Huber, C., Bachmann, O., and Dufek, J., 2011, Thermo-mechanical reactivation of locked crystal mushes: Melting-induced internal fracturing and assimilation processes in magmas: Earth and Planetary Science Letters, v. 304, p. 443–454, doi:10.1016/j.epsl.2011.02.022.

Jagoutz, O., and Behn, M.D., 2013, Foundering of lower island-arc crust as an explanation for the origin of the continental Moho: Nature, v. 504, p. 131–134, doi:10.1038/nature12758.

Jagoutz O., and Kelemen P.B., 2015, Role of arc processes in the formation of continental crust: Annual Reviews of Earth and Planetary Science, v. 43, p. 12.1–12.4, doi:10.1146/annurev-earth-040809-152345.

Jamieson, R.A., and Beaumont, C., 2011, Coeval thrusting and extension during lower crustal ductile flow—Implications for exhumation of high-grade metamorphic rocks: Journal of Metamorphic Geology, v. 29, p. 33–51, doi:10.1111/j.1525-1314.2010.00908.x.

Kay, R.W., and Kay, S.M., 1993, Delamination and delamination magmatism: Tectonophysics, v. 219, p. 177–189, doi:10.1016/0040-1951(93)90295-U.

Kidder, S., Ducea, M.N., Gehrels, G., Patchett, P.J., and Vervoort, J., 2003, Tectonic and magmatic development of the Salinian Coast Ridge Belt, California: Tectonics, v. 22, no. 5, p. 1058, doi:10.1029/2002TC001409.

Kim, J., Gale, M., Thompson, P., and Derman, K., 2007, Bedrock Geologic Map of the Town of Williston, Vermont: Vermont Geological Survey Open-File Report VG07-4, scale 1:24,000.

King, D.S., Klepeis, K.A., Goldstein, A.G., Gehrels, G.E., and Clarke, G.L., 2008, The initiation and evolution of the transpressional Straight River shear zone, central Fiordland, New Zealand: Journal of Structural Geology, v. 30, p. 410–430, doi:10.1016/j.jsg.2007.12.004.

Klepeis, K.A., Clarke, G.L., Gehrels, G., and Vervoort, J., 2004, Processes controlling vertical coupling and decoupling between the upper and lower crust of orogens: results from Fiordland, New Zealand: Journal of Structural Geology, v. 26, no. 4, p. 765–791, doi: 10.1016/j.jsg.2003.08.012.

Klepeis, K.A., King, D., De Paoli, M., Clarke, G.L., and Gehrels, G., 2007, Interaction of strong lower and weak middle crust during lithospheric extension in western New Zealand: Tectonics, v. 26, TC4017, doi:10.1029/2006TC002003.

Kretz, R., 1983, Symbols for rock-forming minerals: The American Mineralogist, v. 68, p. 277–279.

Kruckenberg, S.C., Vanderhaeghe, O., Ferré, E.C., Teyssier, C., and Whitney, D.L., 2011, Flow of partially molten crust and the internal dynamics of a migmatite dome, Naxos, Greece: Tectonics, v. 30, p. TC3001, p. 1–24, doi:10.1029/2010TC002751.

Kruckenberg, S.C., Tikoff, B., Toy, V.G., Newman, J., and Young, L.I., 2013, Strain localization associated with channelized melt migration in upper mantle lithosphere: Insights from the Twin Sisters ultramafic complex, Washington, USA: Journal of Structural Geology, v. 50, p. 133–147, doi:10.1016/j.jsg.2012.10.009.

Kula, J.L., Tulloch, A.J., Spell, T.L., and Wells, M.L., 2007, Two-stage rifting of Zealandia-Australia-Antarctica: Evidence from $^{40}Ar/^{39}Ar$ thermochronometry of the Sisters shear zone, Stewart Island, New Zealand: Geology, v. 35, p. 411–414, doi:10.1130/G23432A.1.

Larter, R.D., Cunningham, A.P., Barker, P.F., Gohl, K., and Nitsche, F.O., 2002, Tectonic evolution of the Pacific margin of Antarctica: 1. Late Cretaceous tectonic reconstructions: Journal of Geophysical Research, v. 107, no. B12, p. 2346, doi:10.1029/2000JB000052.

Lee, C.-T.A., 2014, Physics and Chemistry of Deep Continental Crust Recycling, *in* Rudnick, R.L., ed., Treatise on Geochemistry (second edition), Volume 4: The Crust, Elsevier Ltd., p. 423–456, doi:10.1016/B978-0-08-095975-7.00314-4.

Lee, C.T., Cheng, X., and Horodyskyi, U., 2006, The development and refinement of continental arcs by primary basaltic magmatism, garnet pyroxenite accumulation, basaltic recharge and delamination: Insights from the Sierra Nevada, California: Contributions to Mineralogy and Petrology, v. 151, p. 222–242, doi:10.1007/s00410-005-0056-1.

Little, T.A., Hacker, B.R., Gordon, S.M., Baldwin, S.L., Fitzgerald, P.G., Ellis, S., and Korchinski, M., 2011, Diapiric exhumation of Earth's youngest (UHP) eclogites in the gneiss domes of the D'Entrecasteaux Islands, Papua New Guinea: Tectonophysics, v. 510, p. 39–68, doi:10.1016/j.tecto.2011.06.006.

Luyendyk, B.P., 1995, Hypothesis for Cretaceous rifting of East Gondwana caused by subducted slab capture: Geology, v. 23, p. 373–376, doi:10.1130/0091-7613(1995)023<0373:HFCROE>2.3.CO;2.

Marcotte, S.B., Klepeis, K.A., Clarke, G.L., Gehrels, G., and Hollis, J.A., 2005, Intra-arc transpression in the lower crust and its relationship to magmatism in a Mesozoic magmatic arc: Tectonophysics, v. 407, p. 135–163, doi:10.1016/j.tecto.2005.07.007.

McCoy-West, J., Mortimer, N., and Ireland, T.R., 2014, U-Pb geochronology of Permian plutonic rocks, Longwood Range, New Zealand: Implications for Median Batholith–Brook Street terrane relations: New Zealand Journal of Geology and Geophysics, v. 57, no. 1, p. 65–85, doi:10.1080/00288306.2013.869235.

Miller, R.B., Paterson, S.R., and Matzel, J.P., 2009, Plutonism at different crustal levels: Insights from the ~5–40 km (paleodepth) North Cascades crustal section, Washington, *in* Miller, R.B., and Snoke, A.W., eds., Crustal Cross Sections from the Western North American Cordillera and Elsewhere: Implications for Tectonic and Petrologic Processes: Geological Society of America Special Paper 456, p. 125–149.

Mortimer, N., 2008, Zealandia, *in* Spencer, J.E., and Titley, S.R., eds., Ores and Orogenesis: Circum-Pacific Tectonics, Geologic Evolution, and Ore Deposits: Arizona Geological Society Digest, v. 22, p. 227–233.

Mortimer, N., Tulloch, A.J., Spark, R.N., Walker, N.W., Ladley, E., Allibone, A., and Kimbrough, D.L., 1999, Overview of the Median Batholith, New Zealand: A new interpretation of the geology of the Median tectonic zone and adjacent rocks: Journal of African Earth Sciences, v. 29, p. 257–268, doi:10.1016/S0899-5362(99)00095-0.

Mortimer, N., Hoernle, H., Hauff, F., Palin, J.M., Dunlap, W.J., Werner, R., and Faure, K., 2006, New constraints on the age and evolution of the Wishbone Ridge, southwest Pacific Cretaceous microplates, and Zealandia–West Antarctica breakup: Geology, v. 34, no. 3, p. 185–188, doi:10.1130/G22168.1.

Oliver, G.J.H., 1977, Feldspathic hornblende and garnet granulites and associated anorthosite pegmatites from Doubtful Sound, Fiordland, New Zealand: Contributions to Mineralogy and Petrology, v. 65, p. 111–121, doi:10.1007/BF00371051.

Oliver, G.J.H., and Coggon, J.H., 1979, Crustal structure of Fiordland, New Zealand: Tectonophysics, v. 54, p. 253–292, doi:10.1016/0040-1951(79)90371-8.

Otamendi, J.E., Ducea, M.N., and Bergantz, G.W., 2012, Geological, petrological and geochemical evidence for progressive construction of an arc crustal section, Sierra de Valle Fertil, Famatinian Arc, Argentina: Journal of Petrology, v. 53, no. 4, p. 761–800, doi:10.1093/petrology/egr079.

Paterson, S.R., Fowler, T.K., Jr., Schmidt, K.L., Yoshinobu, A.S., Yuan, E.S., and Miller, R.B., 1998, Interpreting magmatic fabric patterns in plutons: Lithos, v. 44, p. 53–82, doi:10.1016/S0024-4937(98)00022-X.

Paterson, S.R., Okaya, D., Memeti, V., Economos, R., and Miller, R.B., 2011, Magma addition and flux calculations of incrementally constructed magma chambers in continental margin arcs: Combined field, geochronologic, and thermal modeling studies: Geosphere, v. 7, p. 1439–1468, doi:10.1130/GES00696.1.

Petford, N., Atherton, M.P., and Halliday, A.N., 1996, Rapid magma production rates, underplating and remelting in the Andes: Isotopic evidence from northern-central Peru (9–11°S): Journal of South American Earth Sciences, v. 9, p. 69–78, doi:10.1016/0895-9811(96)00028-4.

Rey, P., Teyssier, C., and Whitney, D.L., 2009, Extension rates, crustal melting, and core complex dynamics: Geology, v. 37, p. 391–394, doi:10.1130/G25460A.1.

Rey, P., Teyssier, C., Kruckenberg, S.C., and Whitney, D.L., 2011, Viscous collision in channel explains double dome in metamorphic core complexes: Geology, v. 39, p. 387–390, doi:10.1130/G31587.1.

Sadorski, J., 2015, Time Scales of Continental Arc Root Construction and Deep Crustal Magmatic Flux Rates: Insights from U-Pb Zircon Geochronology of a Triassic–Cretaceous Arc, Fiordland, New Zealand [M.S. thesis]: Northridge, California, California State University–Northridge, 372 p.

Sadorski, J.F., Schwartz, J.J., Stowell, H., Klepeis, K., Tulloch, A., and Coble, M.A., 2013, Time scales of continental arc root construction and deep crustal magmatic flux rates: Insights from U-Pb zircon geochronology of a Triassic–Cretaceous arc, Fiordland, New Zealand: Geological Society of America Abstracts with Programs, v. 45, no. 7, p. 391.

Saleeby, J.B., Ducea, M.N., and Clemens-Knott, D., 2003, Production and loss of high-density batholithic roots: Tectonics, v. 22, no. 6, p. 1064, doi:10.1029/2002TC001374.

Schulte, D.O., Ring, U., Thomson, S.N., Glodny, J., and Carrad, H., 2014, Two-stage development of the Paparoa metamorphic core complex, West Coast, South Island, New Zealand: Hot continental extension precedes sea-floor spreading by ~25 m.y.: Lithosphere, v. 6, p. 177–194, doi:10.1130/L348.1.

Schwartz, J.J., Stowell, H.H., Klepeis, K.A., Zamora, C., Tulloch, A.J., Kylander-Clark, A.R.C., Hacker, B.R., and Coble, M., 2016, Thermochronology of extensional orogenic collapse in the deep crust, Fiordland, New Zealand: Geosphere (in press), doi:10.1130/GES1232.1.

Scott, J.M., Cooper, A.F., Tulloch, A.J., and Spell, T.L., 2011, Crustal thickening of the Early Cretaceous paleo-Pacific Gondwana margin: Gondwana Research, v. 20, p. 380–394, doi:10.1016/j.gr.2010.10.008.

Siddoway, C.S., Baldwin, S.L., Fitzgerald, P.G., Fanning, C.M., and Luyendyk, B.P., 2004, Ross Sea mylonites and the timing of intracontinental extension within the West Antarctic rift system: Geology, v. 32, no. 1, p. 57–60, doi:10.1130/G20005.1.

Spell, T.L., McDougall, I., and Tulloch, A.J., 2000, Thermochronologic constraints on the breakup of the Pacific Gondwana margin: The Paparoa metamorphic core complex, South Island, New Zealand: Tectonics, v. 19, no. 3, p. 433–451, doi:10.1029/1999TC900046.

Stowell, H., Odom Parker, K., Gatewood, M., Tulloch, A., and Koenig, A., 2014, Temporal links between pluton emplacement, garnet granulite metamorphism, partial melting and extensional collapse in the lower crust of a Cretaceous magmatic arc, Fiordland, New Zealand: Journal of Metamorphic Geology, v. 32, p. 151–175, doi:10.1111/jmg.12064.

Sutherland, R., Barnes, P., and Uruski, C., 2006, Miocene–Recent deformation, surface elevation, and volcanic intrusion of the overriding plate during subduction initiation, offshore southern Fiordland, Puysegur margin, southwest New Zealand: New Zealand Journal of Geology and Geophysics, v. 49, no. 1, p. 131–149, doi:10.1080/00288306.2006.9515154.

Tulloch, A.J., and Kimbrough, D.L., 1989, The Paparoa metamorphic core complex, New Zealand; Cretaceous extension associated with fragmentation of the Pacific margin of Gondwana: Tectonics, v. 8, p. 1217–1235, doi:10.1029/TC008i006p01217.

Tulloch, A.J., and Kimbrough, D.L., 2003, Paired plutonic belts in convergent margins and the development of high Sr/Y magmatism: Peninsular Ranges Batholith of Baja-California and Median Batholith of New Zealand, *in* Johnson, S.E., Paterson, S.R., Fletcher, J.M., Girty, G.H., Kimbrough, D.L., and Martín-Barajas, A., eds., Tectonic Evolution of Northwestern México and the Southwestern USA: Geological Society of America Special Paper 374, p. 275–295, doi:10.1130/0-8137-2374-4.275.

Tulloch, A.J., Ramezani, J., Mortimer, N., Mortensen, J., van den Bogaard, P., and Maas, R., 2009, Cretaceous felsic volcanism in New Zealand and Lord Howe Rise (Zealandia) as a precursor to final Gondwana breakup, *in* Ring, U., and Wernicke, B., eds., Extending a Continent: Architecture, Rheology and Heat Budget: Geological Society of London Special Publication 321, p. 89–118.

Turnbull, I.M., Allibone, A.H., and Jongens, R., 2010, Geology of the Fiordland Area: Lower Hutt, New Zealand, Institute of Geological and Nuclear Sciences, Sheet 17, scale 1:250,000, 97 p. text.

Vanderhaeghe, O., 2009, Migmatites, granites and orogeny: Flow modes of partially molten rocks and magmas associated with melt/solid segregation in orogenic belts: Tectonophysics, v. 477, p. 119–134, doi:10.1016/j.tecto.2009.06.021.

Vigneresse, J.L., Barbey, P., and Cuney, M., 1996, Rheological transitions during partial melting and crystallization with application to felsic magma segregation and transfer: Journal of Petrology, v. 37, p. 1579–1600, doi:10.1093/petrology/37.6.1579.

Walcott, R.I., 1998, Modes of oblique compression: Late Cenozoic tectonics of the South Island of New Zealand: Reviews of Geophysics, v. 36, p. 1–26, doi:10.1029/97RG03084.

Webber, J.R., Klepeis, K.A., Webb, L.E., Cembrano, J., Morata, D., Mora-Klepeis, G., and Arancibia, G., 2015, Deformation and magma transport in a crystallizing plutonic complex, Coastal Batholith, central Chile: Geosphere, v. 11, no. 5, p. 1401–1426, doi:10.1130/GES01107.1.

Whitney, D.L., Teyssier, C., and Vanderhaeghe, O., 2004, Gneiss domes and crustal flow, *in* Whitney, D.L., Teyssier, C., and Siddoway, C.S., eds., Gneiss Domes in Orogeny: Geological Society of America Special Paper 380, p. 15–33, doi:10.1130/0-8137-2380-9.15.

Yoshinobu, A.S., Wolak, J.M., Paterson, S.R., Pignotta, G.S., and Anderson, H.S., 2009, Determining relative magma and host rock xenolith rheology during magmatic fabric formation in plutons: Examples from the middle and upper crust: Geosphere, v. 5, p. 270–285, doi:10.1130/GES00191.1.

MANUSCRIPT RECEIVED 8 AUGUST 2015
REVISED MANUSCRIPT RECEIVED 15 DECEMBER 2015
MANUSCRIPT ACCEPTED 5 JANUARY 2016

Printed in the USA